

**Development and Characterization of Graphitic Carbon Nanofiber**

by

Zaid Bin Abdullah

Dissertation submitted in partial fulfilment of  
the requirements for the  
Bachelor of Engineering (Hons)  
(Chemical Engineering)

JANUARY 2009

Universiti Teknologi PETRONAS  
Bandar Seri Iskandar  
31750 Tronoh  
Perak Darul Ridzuan

# **CERTIFICATION OF APPROVAL**


## **Development and Characterization of Graphitic Carbon Nanofiber**

by

Zaid bin Abdullah

A project dissertation submitted to the  
Chemical Engineering Programme  
Universiti Teknologi PETRONAS  
in partial fulfilment of the requirement for the  
BACHELOR OF ENGINEERING (Hons)  
(CHEMICAL ENGINEERING)

Approved by,



---

(A.P. Dr. Suzana binti Yusup)

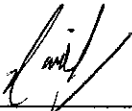
UNIVERSITI TEKNOLOGI PETRONAS

TRONOH, PERAK

APRIL 2009

## **CERTIFICATION OF ORIGINALITY**

This is to certify that I am responsible for the work submitted in this project, that the original work is my own except as specified in the references and acknowledgements, and that the original work contained herein have not been undertaken or done by unspecified sources or persons.



---

ZAID BIN ABDULLAH

## ABSTRACT

The thesis outlines the findings for Final Year Project research entitled “**Development and Characterization of Graphitic Carbon Nanofiber**”. The long-term key objective of the project is to produce carbon nanofiber (CNF) with high surface area, thus allowing high capacity of hydrogen storage. The scope of study covers the process of synthesizing CNF using the already developed metal catalysts, Nickel (Ni) and Iron (Fe) via Chemical Vapor Deposition (CVD) method. The main difference between the author’s research and other existing research is that the catalyst used is of a hybrid composition between both nickel and iron oxide. 3 main factors are varied and studied to synthesize the CNF; hybrid catalyst composition, reaction temperature, and reaction time. After CNF is developed, it is characterized under Scanning Electron Microscopy (SEM), Transmission Electron Microscopy (TEM), X-ray Diffraction (XRD) and Energy Dispersive X-ray Spectroscopy (EDX) for study of the structure morphology and particle size. To further identify the effectiveness of the synthesized CNF, activities to store hydrogen within the material is to be explored.

## ACKNOWLEDGMENT

“Praise to Allah, the most Gracious and the most Merciful”

First and foremost, my deepest gratitude goes for God, for He has guided and blessed me during the whole 2 semesters of final year research, or more accurately, since my early journey in this education institution. I would also like to take this chance to thank my family & friends, for their full support has kept me going from the start until now.

My sincerest gratitude towards my Supervisor, Dr Suzana binti Yusup, for the never ending patience you had to put up with me, and your determination to make me learn as much as I can throughout the research time. Not to forget, I would never had been able to complete such a project if it weren't for the guidance and support from my Co-supervisor, Puan Suriati binti Sufian. My appreciation also goes to the lab technologists from the university, especially from the Chemical and Mechanical Engineering Department, for assisting me in the most helpful manner, and rendering your support every time I needed it.

To all my colleagues, UTP students who are working just as hard to maximize the knowledge and experience here, thank you all for keeping me company, motivated, and learning beside me, so that I don't fall behind. May we continue to be good friends and mingle around even after we graduate as, hopefully, well educated engineers.

To the final year project co-ordinator, thank you for all the arrangements and making success out of this programme for us students.

## TABLE OF CONTENTS

---

<b>ABSTRACT</b> .....	iv
<b>CHAPTER 1: INTRODUCTION</b>	
1.1 Background.....	1
1.2 Problem Statement.....	2
1.3 Objectives and Scope of Study.....	2
<b>CHAPTER 2: LITERATURE REVIEW</b>	
2.1 Theory of Adsorption.....	3
2.2 Carbon Nanomaterials.....	3
2.3 Chemical Vapor Deposition Method.....	7
2.4 Effects of Operating Conditions on Carbon Nanomaterial Growth.....	10
2.5 CNF Characterization.....	13
2.6 Taguchi Method.....	17
<b>CHAPTER 3: METHODOLOGY</b>	
3.1 Process Flow of research Project.....	18
3.2 Development of Carbon Nanofiber.....	20
3.3 Characterization of CNF Structure.....	26
<b>CHAPTER 4: RESULTS &amp; DISCUSSION</b>	
4.1 Yield of CNF formed.....	28
4.2 XRD Pattern.....	30
4.3 Microstructural features of CNF.....	33

4.4.	Chemical Composition of CNF.....	40
4.5.	Main Effect on CNF Yield.....	43
4.6.	Percent Contribution.....	43
<b>CHAPTER 5:</b>	<b>COST ESTIMATION.....</b>	<b>45</b>
<b>CHAPTER 6:</b>	<b>CONCLUSION &amp; RECOMMENDATION.....</b>	<b>46</b>
<b>REFERENCES.....</b>		<b>48</b>
<b>APPENDICES.....</b>		<b>50</b>

## LIST OF FIGURES

Figure 2.1	Schematic of graphite platelets in CNF platelet and herringbone (far-right) structures	4
Figure 2.2	Schematic of graphene walls in CNT structure	5
Figure 2.3	Schematic of carbon nanostructures: (A) platelet CNF, (B) herringbone CNF, (C) multi-walled CNT	5
Figure 2.4	Activated carbon in powder and solid block form	6
Figure 2.5	Schematic diagram of CNF growth on a catalyst particle	8
Figure 2.6	Schematic diagram of CNF growth until carbon encapsulation	9
Figure 2.7	Horizontal tube furnace	9
Figure 2.8	Encapsulated catalyst at 800 °C	12
Figure 2.9	Effect of temperature and feedstock composition on the type of carbon deposited over iron-based catalysts	12
Figure 2.10	Schematic of a SEM	14
Figure 2.11	Schematic of a TEM	14
Figure 2.12	Schematic of diffraction patterns indicative of the crystal structure of CNT, platelet CNF and herringbone CNF	15
Figure 2.13	Schematic of an XRD	16
Figure 2.14	Geometrical representation of Bragg's Law	16
Figure 3.1	Process flow of project research methodology	18
Figure 3.2	Gantt Chart	19
Figure 3.3	Iron (III) oxide (left) and nickel oxide (right) catalyst precursor	20
Figure 3.4	Nickel (left) and iron (right) catalyst preparation from nitrate solution	22
Figure 3.5	Process flow of CNF synthesis via lab experiment	24
Figure 3.6	Schematic diagram of the lab experimental setup	25
Figure 4.1	XRD Graph for Fe-Ni of 1:9	30
Figure 4.2	XRD Graph for Fe-Ni of 1:1	31
Figure 4.3	XRD Graph for Fe-Ni of 9:1	32
Figure 4.4	XRD image of all CNF sample	33
Figure 4.5	SEM image for (A) Fe <sub>1</sub> 4-600-3 and (B) Fe <sub>9</sub> 3-400-8 at 10kX	34



Figure 4.6	SEM image for (A) Fe <sub>13</sub> -500-2 and (B) Fe <sub>52</sub> -500-4 at 10kX	34
Figure 4.7	SEM image for Fe <sub>14</sub> -600-3 at 25kX	35
Figure 4.8	TEM image of Fe <sub>52</sub> -500-4	37
Figure 4.9	TEM image of Fe <sub>92</sub> -600-7	38
Figure 4.10	Encapsulation of catalyst at 600°C for Fe <sub>92</sub> -600-7	39
Figure 4.11	Different compositions of CNF Fe <sub>52</sub> -500-4	40
Figure 4.12	Produced CNF in bulk powder form	42
Figure 4.13	Main effect on yield of CNF	43

## LIST OF TABLES

Table 2.1	Comparison between CNF, CNT, AC and CF characteristics	7
Table 2.2	Comparison of CNF/ CNT growth based on various researches and experiments	10
Table 3.1	Consumables and Equipment for CNF Synthesis	21
Table 3.2	Factors and levels affecting the synthesis of CNF	21
Table 3.3	Experiment design for synthesis of CNF using Taguchi OA L <sub>9</sub>	23
Table 3.4	Equipments for CNF Characterization	26
Table 4.1	Yield of CNF formed from Fe-Ni catalyst	28
Table 4.2	Diameter of CNF formed from Fe-Ni catalyst	36
Table 4.3	Weight percent of CNF composition	41
Table 4.4	Analysis of Variance	44

## **ABBREVIATIONS AND NOMENCLATURES**

CNF	-	Carbon Nanofiber
GNF	-	Graphitic Nanofiber
CNT	-	Carbon Nanotube
AC	-	Activated Carbon
CF	-	Carbon fiber
SEM	-	Scanning Electron Microscopy
EDX	-	Energy Dispersive X-ray Spectroscopy
TEM	-	Transmission Electron Microscopy
XRD	-	X-ray Diffraction
CVD	-	Chemical Vapor Deposition
BET	-	Brunauer, Emmet, Teller
DOE	-	Department of Energy
OA	-	Orthogonal Array
scm	-	standard cubic centimeters per minute
ANOVA	-	Analysis of Variance
H <sub>2</sub>	-	Hydrogen
C <sub>2</sub> H <sub>4</sub>	-	Ethylene
Fe <sub>2</sub> O <sub>3</sub>	-	Iron (III) Oxide
NiO	-	Nickel Oxide

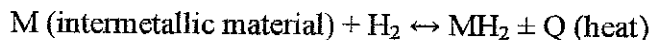
# CHAPTER 1

## INTRODUCTION

### 1.1 Background

Air pollution and global warming are acknowledged among the major crisis in our modern society. Thus, works and researches towards the foundation for renewable and clean energy source are attracting vast attention. A potential energy source, hydrogen, is a candidate fuel for automobile and mobile applications. Hydrogen is not only produced from renewable resources, it has very minimal impact on the environment, and can either be stored as gas, liquid or within a solid medium for transportation purposes [Bououdina, Grant & Walker, 2005].

A solid storage medium for hydrogen is deemed advantageous, due to its operating pressure which is relatively low with regards to safety concerns. A number of intermetallic materials such as  $\text{LaNi}_5$ ,  $\text{ZrMn}_2$ ,  $\text{TiFe}$ , and  $\text{Mg}$  have shown a reversible  $\text{H}_2$  absorption/ desorption with respect to the reaction:



These materials are however too heavy to meet the DOE hydrogen capacity target of 6.5% for onboard mobile transport storage systems [Bououdina et al., 2005].

Recently, activated carbons, carbon nanofibres (CNF) and carbon nanotubes (CNT) have come into attention as potential hydrogen storage materials. Compared to the reversible hydride storage systems where its maximum storage capacities can only reach a weight percent of 1~2 wt%, the storage capacity in CNF is claimed to reach the range of 5~40 wt% at ambient conditions [Blackman, Patrick Arenillas, Wei Shi & Snape, 2006; Gupta, Srivastava, 2000].

Early studies on nanostructured graphite's growth mechanisms involve the decomposition of the hydrocarbon feedstock onto a particular facet of a catalyst, diffusion through the surface of the particle, and precipitation of a filament on another facet of the catalyst particle

[McCaldin, Bououdina, Grant & Walker, 2006]. This method is today more widely known as chemical vapor deposition (CVD), a process which synthesizes CNF over the use of metal catalysts.

## **1.2 Problem Statement**

CNF is a potential solid medium to store hydrogen gas with minimal environmental issues for transportation purposes. Hydrogen is adsorbed on the surface and incorporated between the graphitic sheets of CNF [Bououdina et al., 2005]. To maximize the capacity of CNF's hydrogen storage, it is favorable to synthesize CNF with higher surface area. Such parameters require the control of the operating conditions, as it will further determine the growth of CNF structure. The project should be able to establish an optimum operating condition to construct an efficient CNF structure for maximum storage capacity.

## **1.3 Objectives and Scope of Study**

The main objectives of this research project are as per the following:

- To optimize the synthesis of CNF from the developed hybrid catalyst
- To characterize the developed CNF
- To determine the optimum operating conditions for synthesis of CNF

The scope of the project study covers the synthesis of CNF via CVD method in which the already optimized metal catalyst is used in a hybrid form. The process is optimized by manipulating the reaction conditions during CNF synthesis in reactor. Upon completion, the research is proceeded with the characterization of the developed CNF to study the morphology structure and determine the optimum operating conditions.

## CHAPTER 2

### LITERATURE REVIEW

#### 2.1 Theory of Adsorption

Adsorption phenomena have been known to mankind for a long time, and they are increasingly utilized to perform desired bulk separation, purification purposes, and where this research project is concerned, to allow hydrogen adsorption in CNF as a measure of energy storage. The heart of an adsorption process is usually a porous solid medium, where the porous solid simply provides high surface area or high micropore volume, or in other words, high adsorptive capacity [Duong, 1998].

To further understand the relevance of this subject, adsorption can be defined as a separation of components in a fluid mixture by the transfer of one or more components (the adsorbate) to the internal surface of a porous solid (the adsorbent) where they are held by intermolecular forces [Geankoplis, 2003].

Recently, gas adsorption exhibited by CNFs, have attracted attention as a potential hydrogen storage material. Theoretically, hydrogen is adsorbed on sheets of CNF/GNFs. The space between the sheets which is  $\geq 3.35 \text{ \AA}$ , acts like a slit-shaped pore hence enabling CNFs to physisorb large amounts of hydrogen. Theoretically, the kinetic diameter of a hydrogen molecule is only  $2.89 \text{ \AA}$  [Bououdina et al., 2005].

#### 2.2 Carbon Nanomaterials

In recent years, the detailed structure of filamentous graphite has been closely investigated and researched, credits to the advancement in electron microscopy. Hence, two different types of filamentous nanostructured graphite have been characterized:

- Carbon nanofibers (CNF)
- Carbon nanotubes (CNT)

### 2.2.1 Carbon nanofibers and carbon nanotubes

CNF, also known as graphitic nanofiber (GNF), belongs to carbon nanostructures based on graphite. The basic microstructure consists of stacked graphite layers, which can be arranged parallel/ perpendicular to the fiber axis, or herringbone structure, often with an amorphous component [Bououdina et al., 2005].

Further classification shows that graphite platelets are perpendicular to the fiber axis in platelet/stacked form, while graphene platelets are at an angle to the fiber axis in herringbone form. The stacked and herringbone CNF are associated with energy storage applications such as electrodes for lithium batteries or fuel cells as small ions/ molecules can enter via open-edges and intercalate between the graphene layers [Teo, Singh, Chhowalla & Milne, 2003].

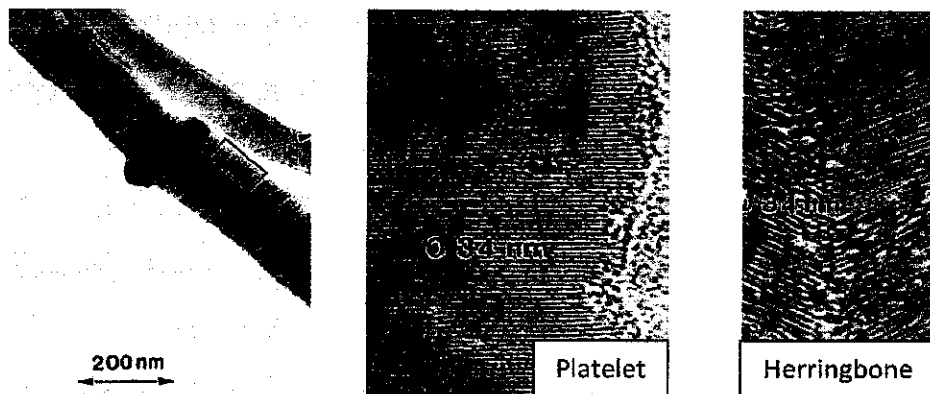


**FIGURE 2.1:** Schematic of graphite platelets in CNF platelet and herringbone (far-right) structures [Teo et al., 2003]

For nanotube structures, the graphene walls, which can either be categorized as single or multi-walled, are parallel to the fiber axis. The highly crystallized tubular carbon structures inherit important properties of “intraplane” graphite, where CNT exhibits high electrical conductivity, thermal conductivity, and mechanical strength along its axis [Teo et al., 2003].

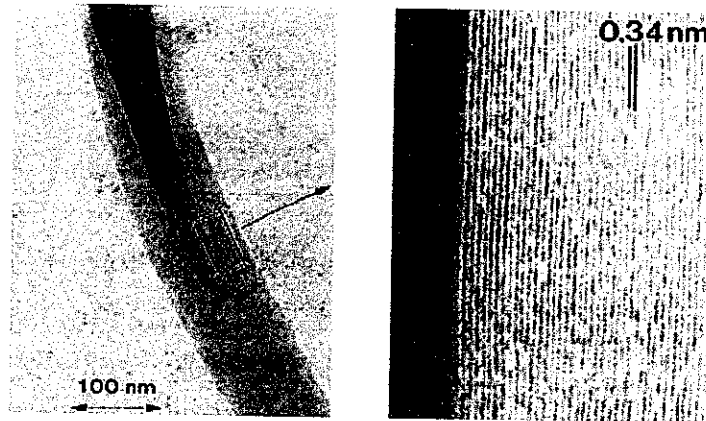


**FIGURE 2.2:** Schematic of graphene walls in CNT structure [Teo et al., 2003]

To easily distinguish the difference between CNF and CNT structures, the following Figure 2.3 shows the position of each graphene layers for both carbon nanomaterials respectively.

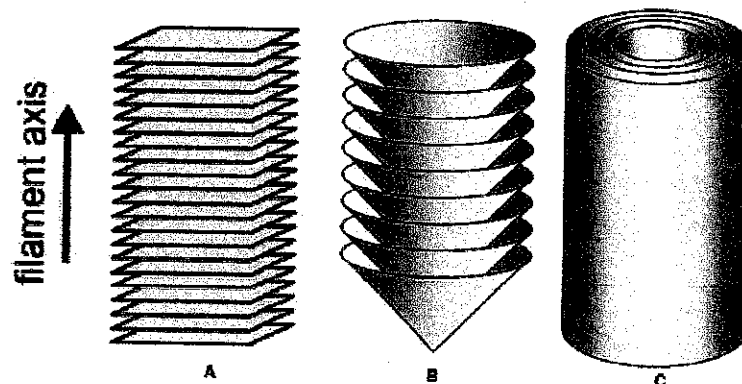


**FIGURE 2.3:** Schematic of carbon nanostructures: (A) platelet CNF, (B) herringbone CNF, (C) multi-walled CNT [McCaldin et al., 2006; Teo et al., 2003]

### 2.2.2 Activated Carbon

Apart from other practical solids used in industries, activated carbon is one of the most complex but versatile solids due to its extremely high surface area and micropore volume.

One of its important structures is graphitic as opposed to amorphous structure. Graphitic structure provides storage space in the form of slit-shaped channel to accommodate

molecules. For gas-phase separation, typical characteristics of activated carbon include a specific area of 1200 m<sup>2</sup>/g and 800 nm of mean macropore radius [Duong, 1998].



**FIGURE 2.4:** Activated carbon in powder and solid block form [16]

### **2.2.3 Carbon Fiber**

Carbon fibers (CF) refer to fibers with at least 92 wt. % of carbon in composition. Categorized into short or continuous, the available structures are further identified as crystalline, amorphous or partly crystalline. CFs with high proportion of graphite are known as graphite fibers with polycrystalline structure. CFs are commercially available in 3 categories; general-purpose (GP), high-performance (HP) and activated carbon fiber (ACF). GP CFs have amorphous and isotropic structures with low tensile strength and modulus, therefore their cost is cheaper. HP CFs are relatively higher in tensile strength and modulus, while ACF is associated with the presence of large number of open micropores, acting as adsorption sites.

Each category is unique, and has respective applications in the industry. For example, HP CF with polymer-matrix composites is used to manufacture lightweight aircraft. CFs are either fabricated from pitch fiber, polymer fiber, or carbonaceous gasses [Chung, 1994].



**TABLE 2.1:** Comparison between CNF, CNT, AC and CF characteristics [Teo et al., 2003; Duong, 1998; Chung, 1994]

	Carbon Nanofiber	Carbon Nanotube	Activated Carbon	Carbon Fiber
Structure	<ul style="list-style-type: none"> <li>▪ Stacked graphite layers</li> <li>▪ Defective structures</li> </ul>	<ul style="list-style-type: none"> <li>▪ Highly crystallized tubular structures</li> </ul>	<ul style="list-style-type: none"> <li>▪ Amorphous or Graphite-like microcrystalline structure</li> </ul>	<ul style="list-style-type: none"> <li>▪ Crystalline</li> <li>▪ Amorphous or Partly amorphous</li> </ul>
Sub-group	<ul style="list-style-type: none"> <li>▪ Platelet</li> <li>▪ Herringbone</li> </ul>	<ul style="list-style-type: none"> <li>▪ Single wall</li> <li>▪ Double wall</li> <li>▪ Multi wall</li> </ul>	<ul style="list-style-type: none"> <li>▪ Macropore (A)</li> <li>▪ Mesopore (B)</li> <li>▪ Micropore (C)</li> </ul>	<ul style="list-style-type: none"> <li>▪ GP</li> <li>▪ HP</li> <li>▪ Activated CF</li> </ul>
Size/ Diameter	<ul style="list-style-type: none"> <li>▪ Dia. &gt; 20 nm</li> </ul>	<ul style="list-style-type: none"> <li>▪ Dia. &lt; 20 nm</li> </ul>	Sizes: <ul style="list-style-type: none"> <li>▪ A) &gt; 100 nm</li> <li>▪ B) 2 – 100 nm</li> <li>▪ C) &lt; 2 nm</li> </ul>	<ul style="list-style-type: none"> <li>▪ Commercial CF, Dia. : 4 – 15 <math>\mu\text{m}</math> (<math>\geq 4000</math> nm)</li> </ul>
Synthesis	<ul style="list-style-type: none"> <li>▪ Catalytic CVD</li> <li>▪ Microwave Plasma CVD</li> </ul>	<ul style="list-style-type: none"> <li>▪ Catalytic CVD</li> <li>▪ Arc discharge</li> <li>▪ Laser ablation</li> <li>▪ Plasma enhanced CVD</li> </ul>	<ul style="list-style-type: none"> <li>▪ Coal activation by air</li> <li>▪ Gassification by water vapor</li> </ul>	<ul style="list-style-type: none"> <li>▪ PAN polymerization</li> <li>▪ PITCH preparation</li> <li>▪ Catalytic growth</li> </ul>
Function (s)	<ul style="list-style-type: none"> <li>▪ Energy storage</li> <li>▪ Battery electrode filler</li> </ul>	<ul style="list-style-type: none"> <li>▪ Field emission display</li> <li>▪ X-ray tubes</li> </ul>	<ul style="list-style-type: none"> <li>▪ Solvent removal from air</li> <li>▪ Wastewater treatment</li> </ul>	<ul style="list-style-type: none"> <li>▪ GP – concrete reinforcement</li> <li>▪ HP – aircraft lightweight structure</li> </ul>

The above Table 2.1 provides the differences between CNF, CNT, AC and CF. Although all four materials consist of carbon composition, each of them are unique in different ways. The project research will focus on CNF as the potential storage medium for hydrogen. Based on the comparison, CNF differs with CF significantly in terms of its diameter. Nanostructures are often associated with materials having size/ diameter in the nanometer, nm range, as opposed to CF which has the diameter range within micrometer,  $\mu\text{m}$  units.

### 2.3 Chemical Vapor Deposition Method

Today, CNF is commonly synthesized from chemical vapor deposition (CVD) of carbon containing gasses over transition metal catalyst such as Iron, Nickel, Cobalt, Copper etc. The gaseous carbon, for example hydrocarbon, is initially absorbed and decomposed on a

particular facet of the metal catalyst particle. Carbon particles produced from decomposition will dissolve and diffuse through the catalyst particle, and are deposited at the other rear facet of the metal catalyst particle in the form of CNF [13].

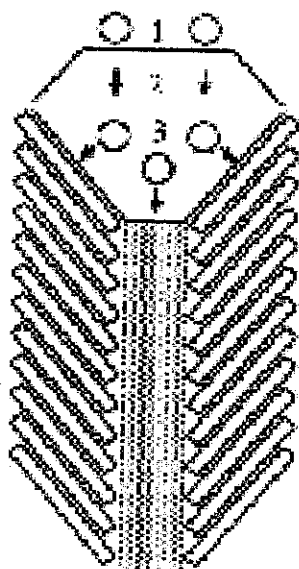


**FIGURE 2.5:** Schematic diagram of CNF growth on a catalyst particle [Blackman, 2005]

Key steps in the growth of a CNF structure [Blackman, 2005]:

1. Adsorption and decomposition of hydrocarbon gas at the particle-gas interface on the front face of the catalyst particle
2. Diffusion of carbon through the catalyst particle
3. Precipitation of carbon at the particle-nanofiber interface on the rear face of the catalyst particle

If the reaction conditions are kept constant, CNF structure continues to grow uninterruptedly, and ceases upon carbon encapsulation of the leading face of the particle. The build-up of the carbon layer prevents further hydrocarbon decomposition.

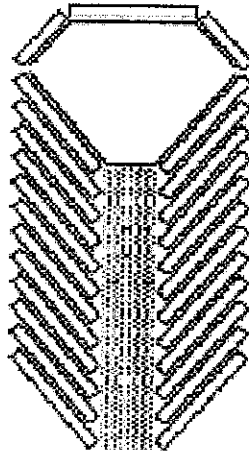


**FIGURE 2.6:** Schematic diagram of CNF growth until carbon encapsulation [Blackman, 2005]

For the project research, a horizontal furnace will be used to run the catalytic CVD process, due to its availability and other advantages which include no (or small) temperature gradient within the heated zone. A typical horizontal furnace is a heated quartz tube in which the catalyst is placed. Upon reaching the desired temperature for the reaction, the reactant gasses are flowed over the catalyst located in a removable ceramic boat/ holder in the centre of the quartz tube [Teo et al., 2003].

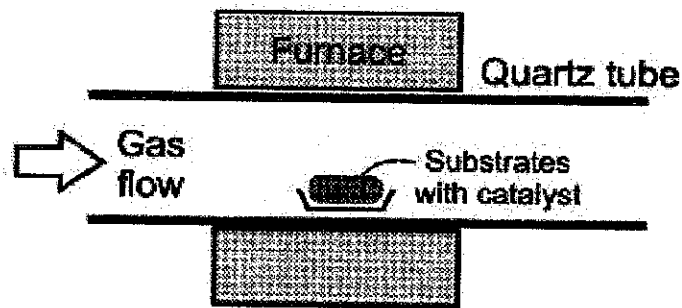


**FIGURE 2.7:** Horizontal tube furnace [Teo et al., 2003]

## 2.4 Effects of operating conditions on carbon nanomaterial growth

Due to the fact that carbon nanomaterials such as CNF/ CNT growth are highly dependent on catalyst type and reaction conditions, a study of different researches and experiments conducted by other scholars have been compiled for further understanding of these parameters.

**TABLE 2.2:** Comparison of CNF/ CNT growth based on various researches and experiments [1, 2, 3, 4, 6]

Ref. No	Author/ Source Journal	Reactor	Catalyst	Feedstock Gas	Reaction Condition	Synthesized structure
1	<i>Effect of processing conditions on unsupported Ni-based catalysts for CNF formation</i>					
	M. Bououdina, D. Grant, G. Walker/ Carbon 43 (2005) 1286-1292	Tube furnace	NiO	C <sub>2</sub> H <sub>4</sub> /H <sub>2</sub> at 80:20 (4:1) (100sccm)	Time: 2 hrs Temp: - 350 °C - 400 °C - 500 °C - 600 °C - 700 °C	CNF: - Herringbone - Herringbone - Platelet - Platelet - Platelet
2	<i>Activation of CNF for H<sub>2</sub> storage</i>					
	James M. Blackman, John W. Patrick, Ana Arenillas, Wei Shi, Colin E. Snape/ Carbon 44 (2006) 1376-1385	Horizontal quartz reactor tube	Copper- nickel, Cu <sub>20</sub> Ni <sub>80</sub> and Iron- nickel, Fe <sub>20</sub> Ni <sub>80</sub> (50mg)	C <sub>2</sub> H <sub>4</sub> /H <sub>2</sub> at 60:240ml/min, (1:4) H <sub>2</sub> flow at 100ml/min, 450°C	Time: 3 hrs Temp: 600°C	Cu <sub>20</sub> Ni <sub>80</sub> : Long CNF with 20µm in excess Fe <sub>20</sub> Ni <sub>80</sub> : Short CNF with max length of 5µm
3	<i>Synthesis and hydrogenation behavior of graphitic nanofibres</i>					
	Bipin Kumar Gupta, O.N. Srivastava/ Int. Journal of Hydrogen Energy 25 (2000) 825-830	Silica tube (75cm long, 2cm diameter)	Fine Ni:Cu at 98:2% (100mg) - passivation	C <sub>2</sub> H <sub>4</sub> /H <sub>2</sub> at 4:1 C <sub>2</sub> H <sub>2</sub> /H <sub>2</sub> at 2:1	Time: 2 hrs Temp: 600°C Pressure: 160torr @ 0.213bar	CNF 1.75gm in 5-6 runs
4	<i>The effect of processing conditions on carbon nanostructures formed on an iron-based catalyst</i>					
	S. McCaldin, M. Bououdina, D.M. Grant, G.S. Walker/ Carbon 44 (2006) 2273-2280	Controlled environment horizontal tube furnace	Fe <sub>2</sub> O <sub>3</sub> precursor (50mg) - Calcined at 300°C, 3 hrs	C <sub>2</sub> H <sub>4</sub> /H <sub>2</sub> at - 100:0 - 80:20,4:1 - 50:50 - <b>20:80,1:4</b> - 5:95 (100sccm)	Time: 2 hrs Temp: - 500 °C - 600 °C - 700 °C - 800 °C	For C <sub>2</sub> H <sub>4</sub> /H <sub>2</sub> at 1:4 - Hergb. CNF - Platelet CNF - MW CNT - Encap.

Ref. No	Author/ Source Journal	Reactor	Catalyst	Feedstock Gas	Reaction Condition	Synthesized structure
5	<i>Structural characterization of carbon nanofibers formed from different carbon-containing gasses</i>					
	Jing-Hong Zhou, Zhi-Jun Sui, Ping Li, De Chen, Ying-Chun Dai, Wei-Kang Yuan/ Carbon 44 (2006) 3255-3262	Fixed-bed quartz reactor	<ul style="list-style-type: none"> <li>- Fe powder</li> <li>- Ni/ Al<sub>2</sub>O<sub>3</sub></li> <li>- NiFe/Al<sub>2</sub>O<sub>3</sub></li> <li>- Ni<sub>3</sub>Fe<sub>2</sub>/Al<sub>2</sub>O<sub>3</sub></li> <li>- Ni<sub>3</sub>Fe<sub>2</sub>/Al<sub>2</sub>O<sub>3</sub></li> <li>- Ni<sub>3</sub>Fe<sub>2</sub>/Al<sub>2</sub>O<sub>3</sub></li> <li>- Ni/ Al<sub>2</sub>O<sub>3</sub></li> </ul>	<ul style="list-style-type: none"> <li>- CO/H<sub>2</sub> <sup>(80:20)</sup></li> <li>- CO/H<sub>2</sub> <sup>(80:20)</sup></li> <li>- CO/H<sub>2</sub> <sup>(80:20)</sup></li> <li>- CO/H<sub>2</sub> <sup>(80:20)</sup></li> <li>- CH<sub>4</sub>/H<sub>2</sub> <sup>(80:10)</sup></li> <li>- C<sub>2</sub>H<sub>4</sub>/H<sub>2</sub> <sup>(40:20)</sup></li> <li>- CH<sub>4</sub>/H<sub>2</sub> <sup>(80:10)</sup></li> </ul>	Time: - 16hr - 24hr - 16hr - 24hr - 24hr - 24hr - 24hr - 24hr Temp: 600°C	CNF yield: - 20.3 g/g <sub>cat</sub> - 19.0 g/g <sub>cat</sub> - 14.3 g/g <sub>cat</sub> - 20.2 g/g <sub>cat</sub> - 25.1 g/g <sub>cat</sub> - 23.2 g/g <sub>cat</sub> - 21.0 g/g <sub>cat</sub>

Table 2.2 shows the different carbon nanomaterials synthesized when different types of catalyst and reaction conditions were adapted during the experiment. All the CNF/ CNT were synthesized using catalytic CVD method. A common reactor used is the horizontal tube furnace where no (or small) temperature gradient occurs within the heated zone [Teo et al., 2003], thus allowing better heat distribution and temperature control during reaction. Most of the CNFs are formed from the use of Fe and Ni as the catalyst, where both will be used for this research study.

Various feedstock gasses (carbon containing gasses) were used in the experiment, including CO, CH<sub>4</sub>, C<sub>2</sub>H<sub>2</sub> and C<sub>2</sub>H<sub>4</sub>, where ethylene, C<sub>2</sub>H<sub>4</sub> is most commonly used with the presence of Ni and Fe-based catalysts, as well as generating among the highest yield of CNF [J.H. Zhou, Z.J. Sui, P. Li, D. Chen, Y.C. Dai & W.K. Yuan, 2006]. For Ni-based catalyst, the composition of carbonaceous gas such as C<sub>2</sub>H<sub>4</sub> is higher than hydrogen feedstock with a ratio of 4:1, as opposed to Fe-based catalyst where hydrogen composition practically overcomes that of C<sub>2</sub>H<sub>4</sub>.

Important operating conditions include temperature and time duration of reaction in furnace. For Ni and Fe-oxide catalysts, the practical temperature is within 350-700 °C, due to encapsulation which occurs around 800 °C when catalysts particles are encased by a layer of carbon and no filamentous carbon has formed (Figure 2.8). Time duration ranges from 2-3 hrs [1, 2, 3, 4], and even up to 24 hours [Zhou et al., 2006], however most of the reaction takes place within 2 hours of reaction.

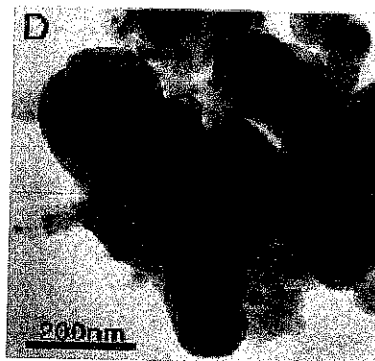


FIGURE 2.8: Encapsulated catalyst at 800 °C [McCaldin et al., 2006]

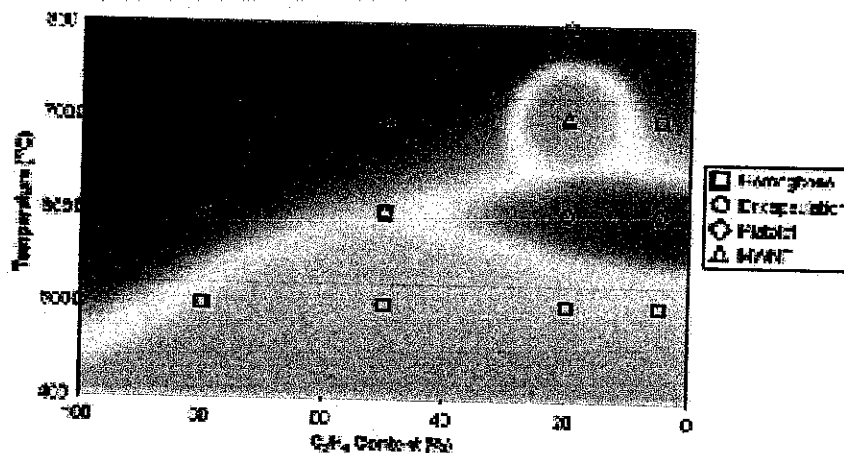


FIGURE 2.9: Effect of temperature and feedstock composition on the type of carbon deposited over iron-based catalysts [McCaldin et al., 2006]

Figure 2.9 above shows the effect of temperature and C<sub>2</sub>H<sub>4</sub> composition against hydrogen gas when Fe is used as a catalyst. At temperature as low as 500 °C, CNF herringbone structure is easily formed, except when 100% C<sub>2</sub>H<sub>4</sub> is used which promotes encapsulation. The temperature increase to 600 °C shows a tendency for platelet CNF structure. Higher temperature of 700 °C initiates encapsulation of catalyst, except when 20% C<sub>2</sub>H<sub>4</sub> is used against 80% hydrogen where MWNT forms. Based on the conducted research, high carbonaceous gas composition promotes encapsulation with a Fe-based catalyst, and high temperature is favorable for CNT structures, before encapsulation occurs at 700-800 °C [McCaldin et al., 2006].

## 2.5 CNF Characterization

For the purpose of studying the physical characteristics of CNF structure produced from the experiments, a series of characterization is to be developed in a way that the microstructures of the CNF are identified. Charged species namely electrons, may be refracted easily using magnetic fields prior to forming an image. Apart from that, X-rays are also capable of handling higher resolution images.

Later technology has introduced electron microscopes, which are able to address the limitations of optical microscopy. To examine objects to a very high resolution, electron microscope employs a beam of highly energetic electrons. This equipment yields a number of information such as the topography, morphology, composition and crystallographic characteristics of nanostructures, and such characterizations are essential to verify the CNF samples.

### 2.5.1. Scanning Electron Microscopy (SEM)

Primarily, SEM yields information of a sample's topography and morphology, and additional equipments able SEM to yield information on composition of the sample in areas as small as  $1 \mu\text{m}^2$ , with the highest achievable resolution of a modern SEM to be approximately 1 nanometer (nm).

Figure 2.10 illustrates the basic design of an SEM. The scanning coils scan the beam in a grid-like fashion, dwelling on points for a period of time with respect to the scan speed, followed by the objective lens which focuses the scanning beam on the sample. Interactions occur once the electron beam strikes the sample, detected by instruments such as secondary and backscatter electron detectors. The number of interactions is counted and a pixel is displayed on a monitor whose intensity is proportional to the count, before the beam moves to its next point. After a repetition of the process, the grid scan completes, and an SEM image is created [Blackman, 2005].

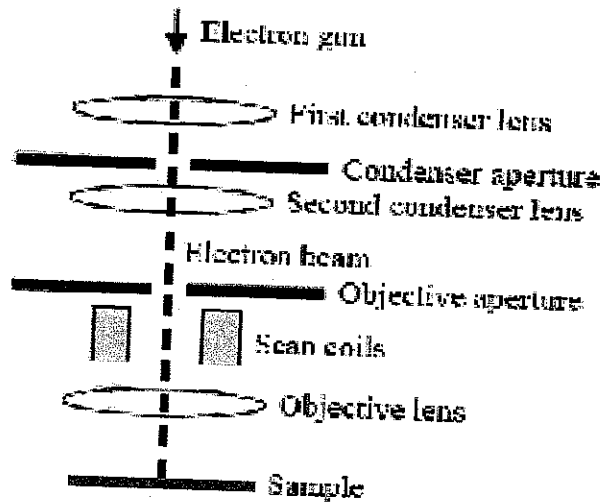


FIGURE 2.10: Schematic of a SEM

### 2.5.2. Transmission Electron Microscopy (TEM)

TEM yields the information of a sample's morphology and crystallography. Able to detect atomic scale in areas of a few nanometers, a modern TEM's highest resolution is sub-nanometer.

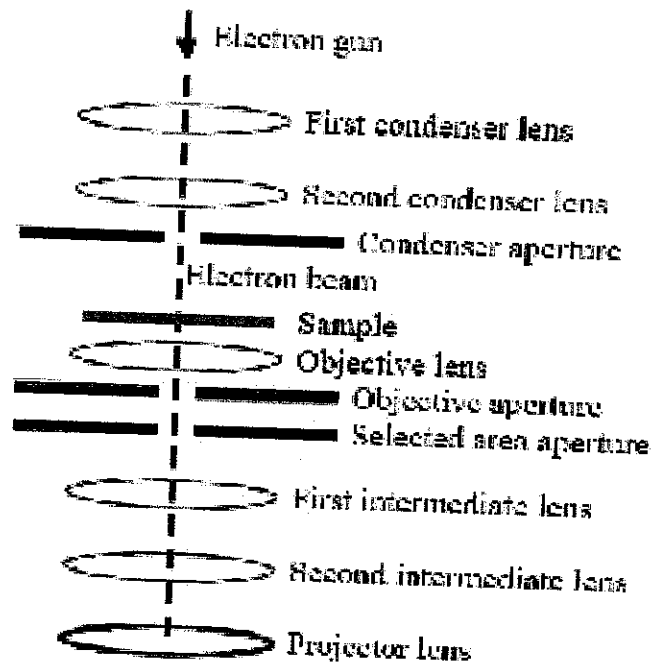
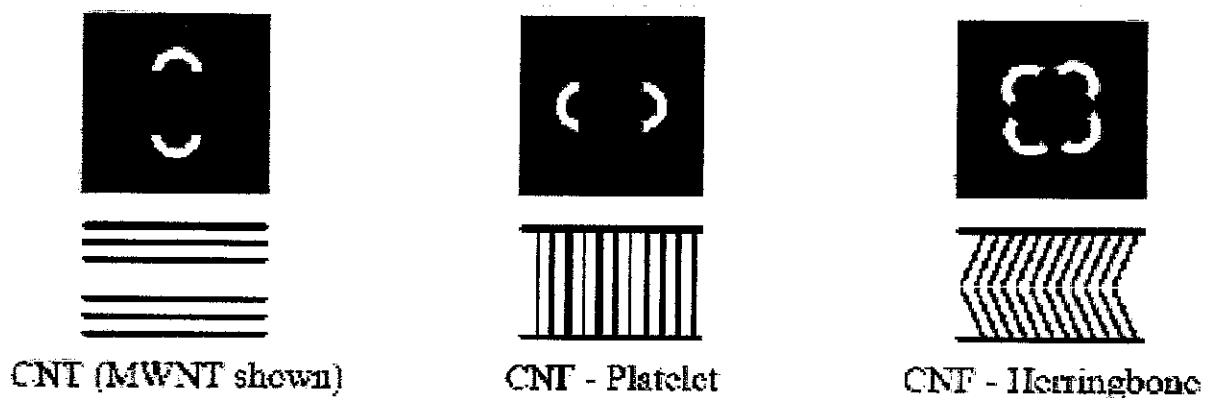


FIGURE 2.11: Schematic of a TEM



The above Figure 2.11 describes the basic schematic of a typical modern TEM. A stream of monochromatic electrons is produced from the electron gun. The condenser lenses focus the beam to a small, thin and coherent beam and the condenser aperture removes high angle electrons. As the electron beam strikes the sample, it is affected by the sample's structure. As a result, only part of the electron beam transmits through certain parts of the sample. The objective aperture enhances the image's contrast by blocking diffracted, high angle electrons, whereas the selected area aperture allows control of the area viewed. The intermediate and projector lenses enlarge the image, and as the beam hits the phosphor image screen, light is generated along with the image. Darker regions of the TEM image represent denser areas of the sample, where fewer electrons were transmitted [Blackman, 2005].

Apart from that, another useful function of TEM includes the ability to focus on the diffraction pattern of the electron beam caused by selected areas of the sample. The pattern yields information of the crystalline structure of the material, which is especially beneficial for the study of CNF and CNT [Blackman, 2005].



**FIGURE 2.12:** Schematic of diffraction patterns indicative of the crystal structure of CNT, platelet CNF and herringbone CNF

### 2.5.3. X-Ray Diffraction (XRD)

XRD pattern of a pure substance is unique, where it utilizes the diffraction of an incident beam of x-rays in order to examine the crystal structure of a material.

The wavelength range of x-rays is comparable to the magnitude of the distance separating ions/ atoms in a crystal, thus causing the crystal to diffract an x-ray beam passing through it. The beams are diffracted by the electron density of a crystal, denoted via the peak in recorded XRD pattern. The crystal structure of the material is deduced from an electron density map of the crystal, created from analysis of the diffracted beams [Blackman, 2005].

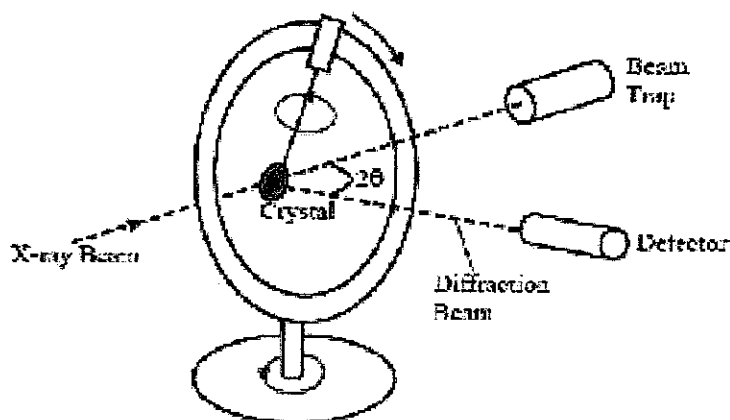


**FIGURE 2.13:** Schematic of an XRD

From Figure 2.13, the beam created by the x-ray generator strikes the sample and is diffracted then detected by either photographic film or a movable proportional counter.

The peaks in an x-ray diffraction pattern are directly related to the atomic distances, explainable with geometry. This relationship is further described by Bragg's law where  $\lambda$  is the wavelength of the x-ray and  $\theta$  the scattering angle;  $\lambda = 2d\sin\theta$  (Figure 2.14) [Blackman, 2005].

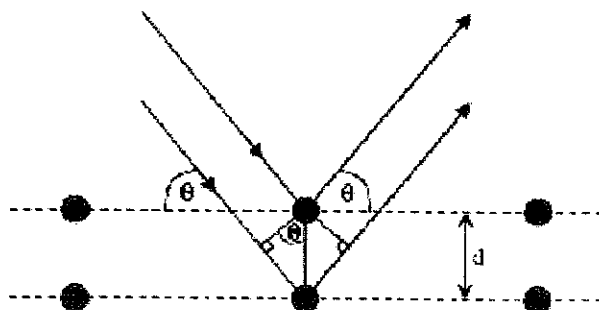


**FIGURE 2.14:** Geometrical representation of Bragg's Law

## 2.6. Taguchi Method

Conventional method of an experiment is that of the common practice in operation, either in lab experiments or at higher production level. In the case of conducting an experiment with 3 factor varied at 3 different levels, the total of the conventional step would take at least 27 sets of experiment.

Taguchi constructed a special set of orthogonal arrays (OA) to lay out his experiments. From 27 sets of experiment, the same number of factors and levels are able to be implemented in only 9 sets, already reducing another 18 sets of trials. For production and researches that costs a lot in terms of raw material or machinery, this reduction is highly important and can significantly reduce the total cost.

Taguchi has provided some key procedures to analyze the result obtained from the experiment. In the Taguchi method the results of the experiments are analyzed to achieve one or more of the following objectives [Roy, 1990]:

- i. To establish the best or the optimum condition for a product or a process
- ii. To estimate the contribution of individual factors
- iii. To estimate the response under the optimum conditions

## CHAPTER 3

### METHODOLOGY

#### 3.1 Process Flow of Research Project

For the purpose of the research project, the reaction conditions during CNF synthesis is studied to optimize the process and obtain CNF at a high yield with high BET specific surface area. The following Figure 3.1 illustrates the process flow of the research method that will ensure to meet the set objectives:

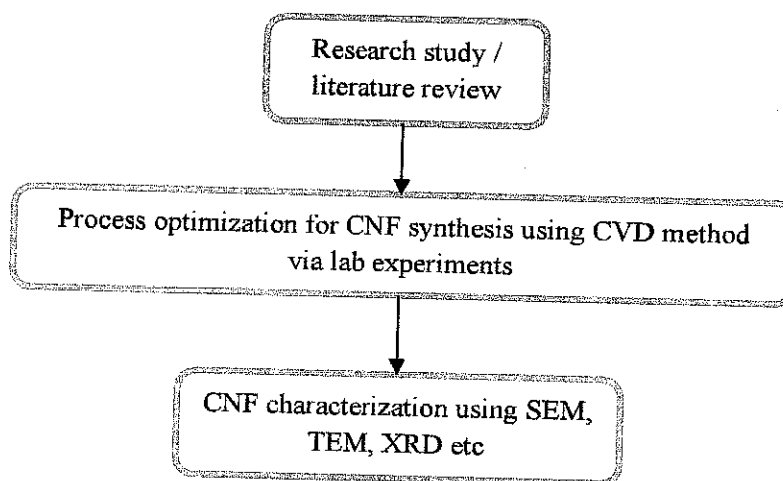
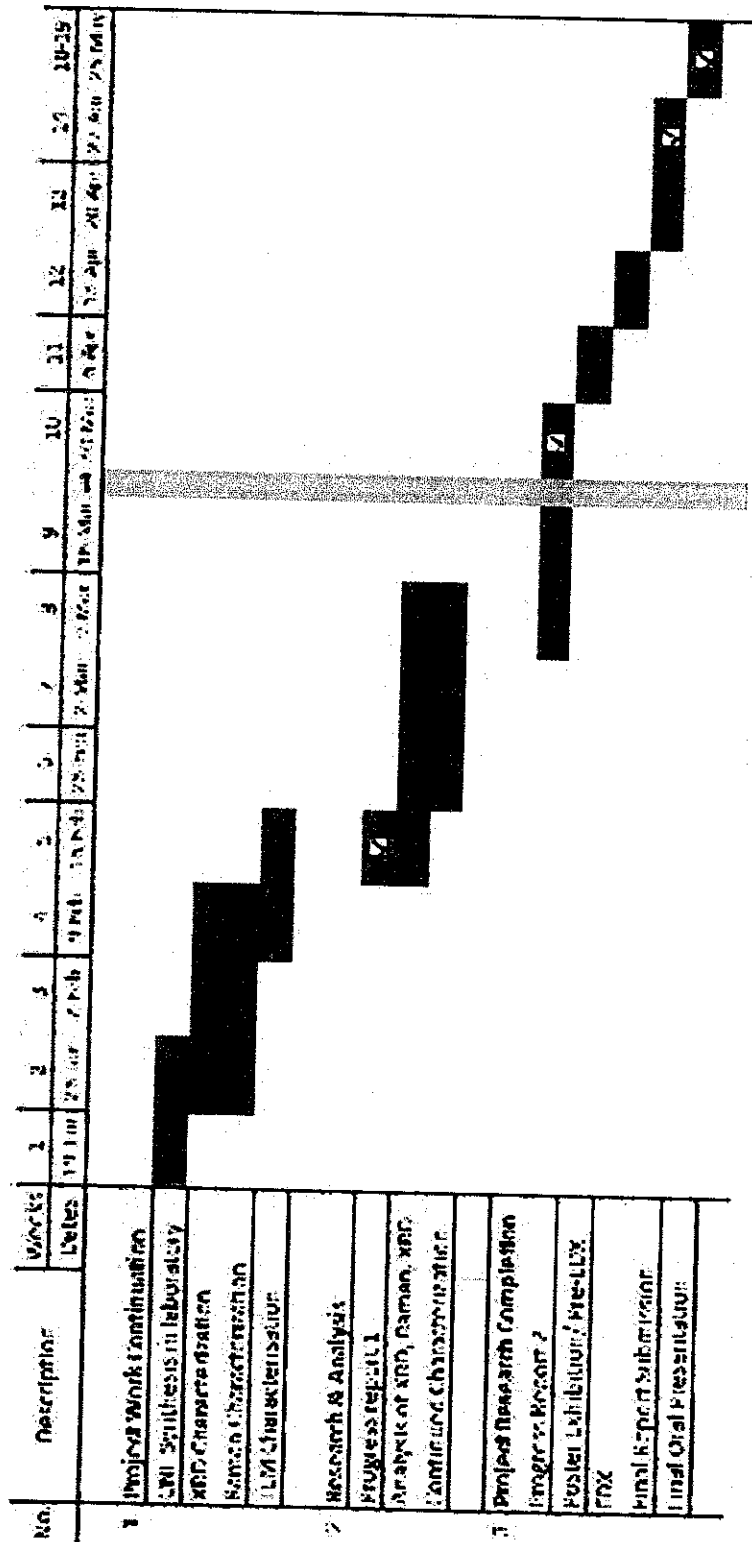


**FIGURE 3.1:** Process flow of project research methodology

The duration of the research project governs the time of approximately 1 year or 2 semesters, starting with research on the literature reviews available to fully understand the project scope and determine the appropriate research methods. Subsequent steps are conducted, which includes synthesizing CNF via laboratory experiments, and further characterization of the developed nanostructures.

Refer to Figure 3.2 for a Gantt Chart of the research project.

Final Year Project II (24-06-14)  
SUNIL KIRAN 2009



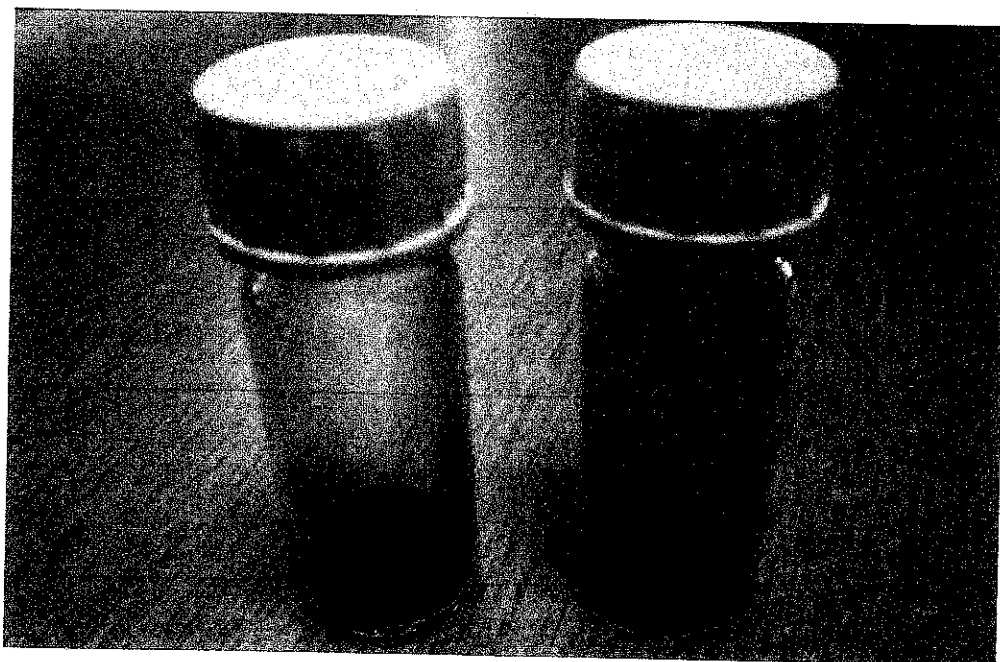
Process  
 Deliverables  
 Milestone (week 22 March 14)

FIGURE 3.2: Gantt Chart

### 3.2 Development of Carbon Nanofiber

A number of methods are available to synthesize CNF. For the purpose of this research project, catalytic CVD method is adapted. As mentioned in the literature review, the gas feedstock can be any carbonaceous gasses such as methane,  $\text{CH}_4$  and ethylene,  $\text{C}_2\text{H}_4$ . Apart from that, available catalyst also varies, such as unsupported Nickel Oxide (NiO), Iron (III) Oxide ( $\text{Fe}_2\text{O}_3$ ) or hybrid catalysts. The selection of gas feedstock will depend on its availability and feasibility; in this case  $\text{C}_2\text{H}_4$  is utilized. Whereas catalyst type for the experiment will prioritize on the already developed unsupported catalysts, NiO and  $\text{Fe}_2\text{O}_3$ . The research project was primarily based on using the catalyst separately, independent of each other in two different sets of experiment. However due to the fact that a similar research is already in progress, further studies on the hybrid catalysts is deemed preferable.

Furthermore, Blackman et al. [2006] and Gupta et al. [2000] reported the usage of a hybrid catalyst between copper and nickel, thus the possibility to produce a high quality CNF structure from hybrid catalysts is not impossible.



**FIGURE 3.3:** Iron (III) oxide (left) and nickel oxide (right) catalyst precursor

In order to perform CNF synthesis, the following consumables/ equipment is used, as per guided in Table 3.1:

**TABLE 3.1: Consumables and Equipment for CNF Synthesis [13]**

Consumables/ Equipment	Function
Ethylene, C <sub>2</sub> H <sub>4</sub>	Source of Carbon, C
Hydrogen, H <sub>2</sub>	Source of hydrogen gas
Argon, Ar	Carrier gas
Nickel Oxide and Iron (III) Oxide	Catalyst
Tube Reactor	To synthesize and develop CNF

### 3.2.1 Selection of factors and levels of experiment

To attain optimum results and consistency, as well as reducing redundancy of unnecessary experiments, Taguchi Method is implemented. The three operating conditions, or in Taguchi Method terms, control factors/parameters are the catalyst composition, reaction time and reaction temperature. Table 3.2 shows the factors and three levels affecting the synthesis of CNF using Taguchi Method:

**TABLE 3.2: Factors and levels affecting the synthesis of CNF**

Factors	Levels		
	Low	Medium	High
Catalyst Composition: Fe-Ni	1/9	5/5	9/1
Reaction time (hour)	2	3	4
Reaction temperature (°C)	400	500	600

Based on literature review, gas composition between C<sub>2</sub>H<sub>4</sub> and H<sub>2</sub> is also significantly important. Due to the fact that a hybrid catalyst of mixed compositions between NiO and Fe<sub>2</sub>O<sub>3</sub> is used, gas composition is fixed at a 1:1 ratio. The main reason for this decision is

that NiO and Fe<sub>2</sub>O<sub>3</sub> both have the opposite favorable composition of carbonaceous gas to hydrogen feedstock to produce non-encapsulated CNF. Thus a constant gas composition is fixed to address both catalyst used at the same time.

The hybrid catalyst is prepared by physically mixing both NiO and Fe<sub>2</sub>O<sub>3</sub> catalysts at the specified composition in a separate container, prior to being placed into the ceramic boat for the reaction process to take place. The compositions are selected at an extreme value, either minimum (1/10 or 1:9 ratio) or maximum (9/10 or 9:1 ratio), to allow a significant effect of each catalyst for each samples.

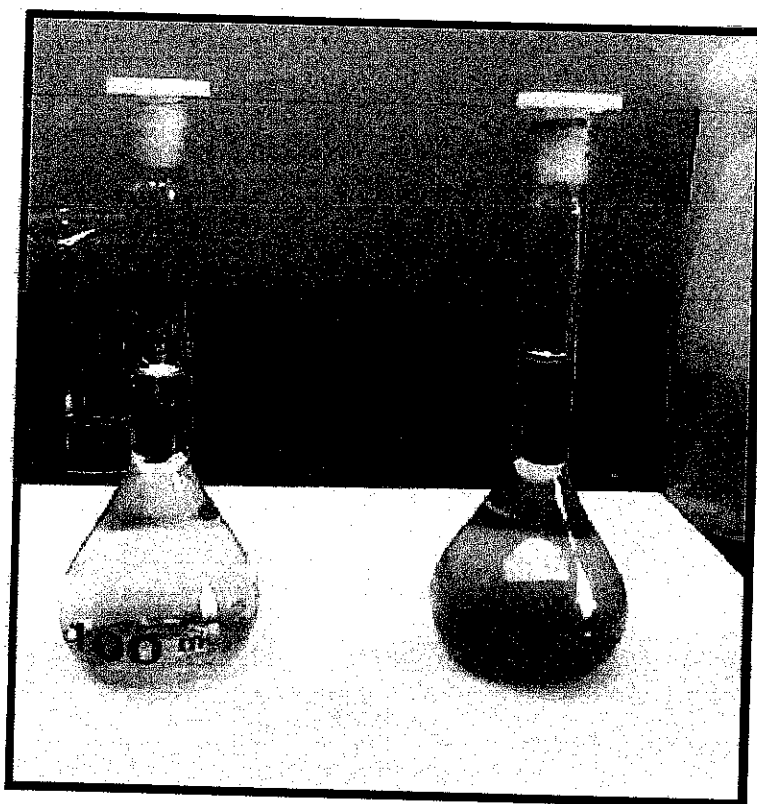


**FIGURE 3.4:** Nickel (left) and iron (right) catalyst preparation from nitrate solution



All factors contain 3 levels and therefore the array is referred to as the 3<sup>n</sup> series. Since 3 factors with 3 levels are to be studied, the orthogonal array L<sub>9</sub> is used [Ross, 1996; Peace, 1993]. The values of each level were determined based on previous researches by other scholars.

**TABLE 3.3:** Experiment design for synthesis of CNF using Taguchi OA L<sub>9</sub>

L <sub>9</sub> (Experiment No.)	Sample Name	Fe-Ni Composition	Reaction Time (hours)	Reaction Temperature (°C)
1	Fe <sub>1</sub> 2-400-1	1/9	2	400
2	Fe <sub>1</sub> 3-500-2	1/9	3	500
3	Fe <sub>1</sub> 4-600-3	1/9	4	600
4	Fe <sub>5</sub> 2-500-4	5/5	2	500
5	Fe <sub>5</sub> 3-600-5	5/5	3	600
6	Fe <sub>5</sub> 4-400-6	5/5	4	400
7	Fe <sub>9</sub> 2-600-7	9/1	2	600
8	Fe <sub>9</sub> 3-400-8	9/1	3	400
9	Fe <sub>9</sub> 4-500-9	9/1	4	500

Table 3.3 shows the designed experiment to synthesize CNF by manipulating the operating conditions; catalyst composition, reaction time and reaction temperature. Each sample is named based on its respective operating condition itself. As previously mentioned, the gas feedstock composition is fixed at a 1:1 ratio. The total gas volume flowed into the reactor is set at 300 ml/min. Thus the flow rate of C<sub>2</sub>H<sub>4</sub> and H<sub>2</sub> are both set at 150ml/min respectively.

### 3.2.2 Experiment Procedure

The following process flow represents the experiment steps to fully develop carbon nanofibers (Figure 3.5):

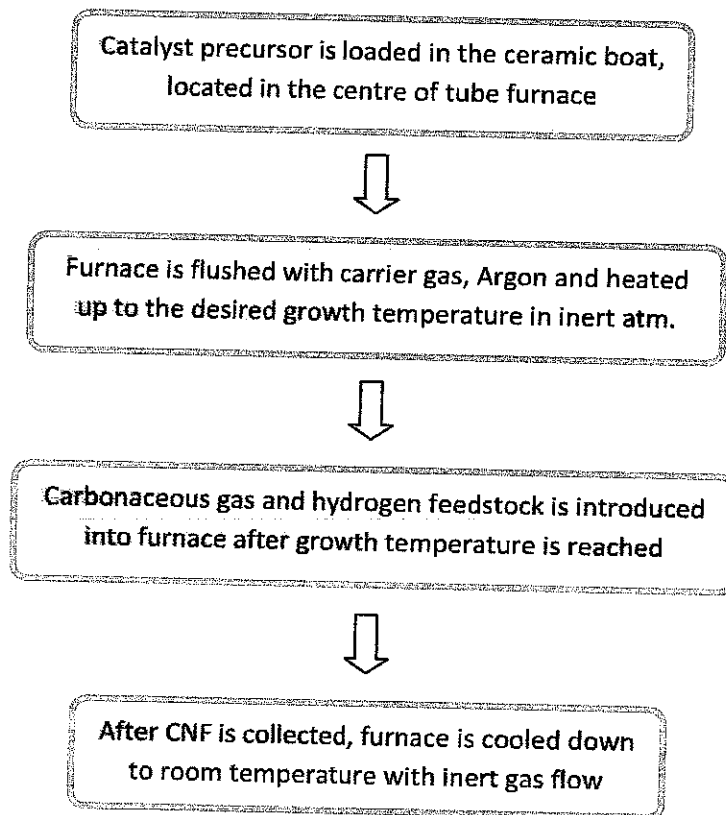


**FIGURE 3.5:** Process flow of CNF synthesis via lab experiment [1, 2, 5]

The following diagram shows the equipment setup for the lab experiments to take place:

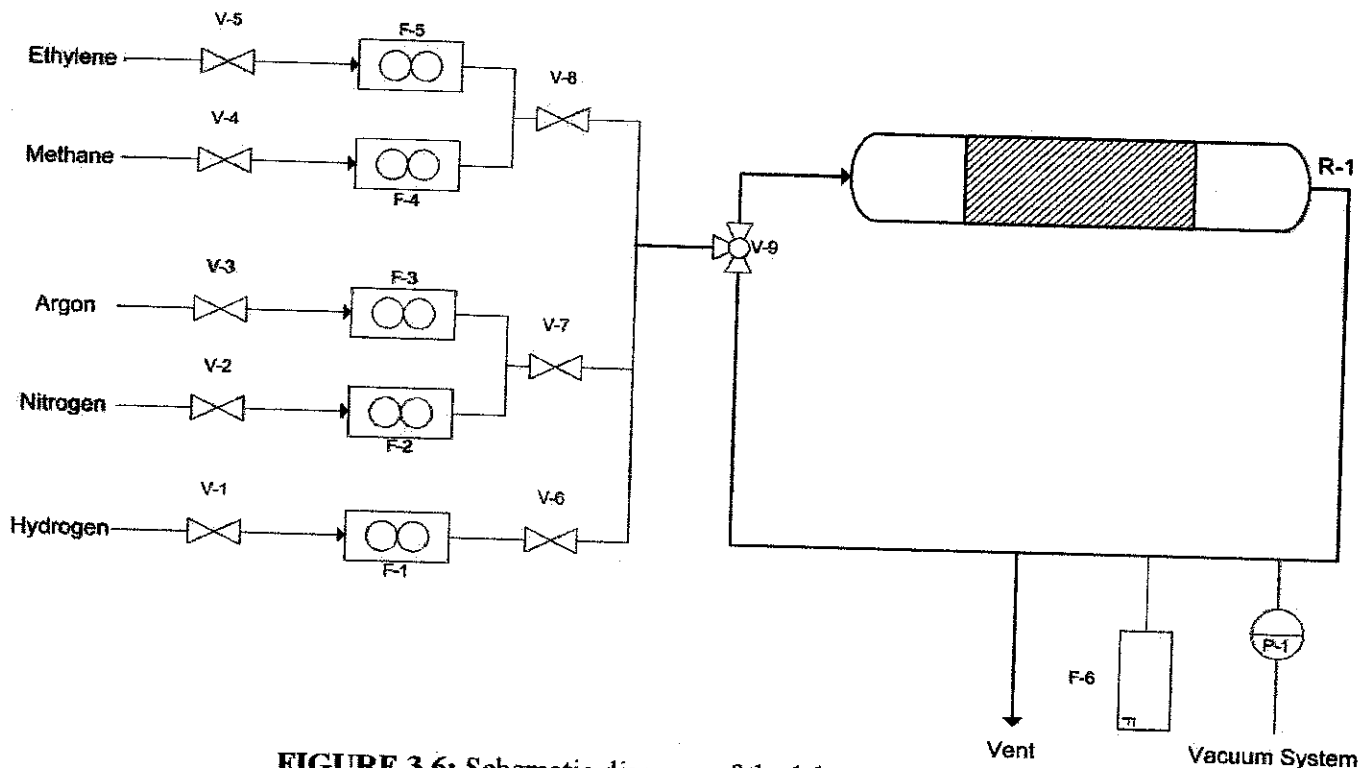


**FIGURE 3.6:** Schematic diagram of the lab experimental setup

**List of diagram:**

- V-1 to V-8: Gate Valve
- V9: 3-way Valve
- F-1 to F-5: Flow meter (gas feedstock)
- F-6: Flow Indicator (reactor outlet)
- R-1: Tubular Reactor
- P-1: Pressure Gauge

The gas feedstock's flow rate into reactor is controlled via valve V-6, V-7, V-8 for hydrogen, argon/nitrogen, and ethylene/methane, respectively. Flow indicator ensures that the activated gas is flowing in the right direction, where the reactor outlet is released via the vent stream without recirculation.

### 3.3 Characterization of CNF structure

#### 3.3.1. Material Characterization

Upon development of CNF structure, the yield of CNF can be estimated using the following equation [Bououdina et al., 2005]:

$$\begin{aligned} \text{Yield of CNF} &= \frac{[g_{\text{CNF}}]}{[g_{\text{catalyst}}][\text{Hour}]} \\ &= g \text{ g}_{\text{cat}}^{-1} \text{ h}^{-1} \end{aligned}$$

For characterization of the CNFs, the following equipments are used as stated in Table 3.4:

TABLE 3.4: Equipments for CNF Characterization [13]

Consumables/ Equipment	Function
Scanning Electron Microscopy (SEM)	Study the micro structural features of material
Transmission Electron Microscopy	Determine the graphitic structure of material
X-ray Diffraction (XRD)	Determine the crystalline structure of material
Raman Spectroscopy	Study the spectra of single crystal/ microcrystalline graphite
Surface Area Analyzer	Determine BET specific surface area of material

Procedures of CNF Characterization [13]:

1. XRD studies are carried out using Bruker AXS D8-Advance diffractometer with Cu  $K\alpha$  radiation of wavelength,  $\lambda = 0.1546 \text{ nm}$ , with operating voltage and current at 40 kV and 40 mA respectively.
2. Each sample is scanned from  $2\theta$  of  $20^\circ$  to  $80^\circ$  and the data is collected in step mode with interval of  $0.02^\circ$ .
3. Scherrer equation is used to estimate the particle sizes.

4. The morphology structure of each sample is studied with Phillips XL30 scanning electron microscope (SEM) at accelerating voltage of 20 kV.
5. SEM is also utilized to perform energy dispersion X-ray (EDX) on the samples to determine the amount of element presented in the sample.

### 3.3.2. Hydrogen Adsorption Characterization

Hydrogen storage capacity is commonly expressed in terms of weight percent (wt %), corresponding to the unit quantity of gas with respect to the sum of the unit quantity of gas and unit quantity of adsorbent. The following equation correlates the relation between both unit quantities [Blackman, 2005]:

$$w = \frac{m_{\text{adsorbate}}}{m_{\text{adsorbent}} + m_{\text{adsorbate}}} \cdot 100$$

From the above equation, w is defined as the weight percent and m is the mass of adsorbate/adsorbent. Other units of measurement that are less common include mol per gram (mol g<sup>-1</sup>) and gram per gram (g g<sup>-1</sup>).

## CHAPTER 4

### RESULTS & DISCUSSION

The CNF structures are developed from the catalytic CVD method, by using different operating conditions in terms of catalyst composition, reaction time, and temperature. Nine series of the experiments are conducted with varying mixture of catalyst, reaction time and reaction temperature, but for the same C<sub>2</sub>H<sub>4</sub> and H<sub>2</sub> gas composition. Based on the CNF produced during the experiments, the yield of each sample can be summarized in the following table:

#### 4.1. Yield of CNF

**TABLE 4.1:** Yield of CNF formed from Fe-Ni catalyst

Sample Name	Fe-Ni Composition	Reaction Time (hour)	Temp. (°C)	Weight of CNF (g)	Yield (g gcat <sup>-1</sup> h <sup>-1</sup> )
Fe <sub>1</sub> 2-400-1	1/9	2	400	0.6793	5.91
Fe <sub>1</sub> 3-500-2	1/9	3	500	4.1002	24.84
Fe <sub>1</sub> 4-600-3	1/9	4	600	9.7307	44.60
Fe <sub>5</sub> 2-500-4	5/5	2	500	1.6644	15.62
Fe <sub>5</sub> 3-600-5	5/5	3	600	3.9144	23.54
Fe <sub>5</sub> 4-400-6	5/5	4	400	0.6510	3.01
Fe <sub>9</sub> 2-600-7	9/1	2	600	0.5692	5.61
Fe <sub>9</sub> 3-400-8	9/1	3	400	0.0763	0.50
Fe <sub>9</sub> 4-500-9	9/1	4	500	0.3478	1.68

Table 4.1 above clarifies the yield obtained for each of the CNF samples. Physically, the CNF produced are in the form of solid black powders, with some of the samples finer than the others. Based on the result of the experiments, each sample is unique, depending on the operating conditions that is set. The 1<sup>st</sup> three samples showed a very obvious trend and dependency on the reaction time and temperature change. To further simplify the trend of the result, it can be categorized into three groups of factor dependency.

Firstly, the gas composition is fixed at 1:1 ratio between  $C_2H_4$  and  $H_2$  (150ml/min each), thus, the type of catalyst used will very much affect the yield and physical structure of the CNF synthesized. Basically, for the particular gas feedstock ratio, higher yield of CNF is produced when the catalyst has a higher composition of NiO, as seen from sample Fe<sub>14</sub>-600-3 with 44.60g/gcat-h. The yield reduces significantly as the composition of Fe<sub>2</sub>O<sub>3</sub> is increased in the hybrid catalyst (sample Fe<sub>9</sub>4-500-9 1.68g/gcat-h). Bououdina et al. [2005] proved that unsupported Ni-based catalyst precursor produces high yield of CNF, as delivered in the author's research.

Secondly, as the reaction time is increased, the yield of CNF produced also increases. Although the effect of reaction time seems less significant, it can still be seen from sample Fe<sub>9</sub>3-400-8 (0.50g/gcat-h in 3 hours reaction time) compared to sample Fe<sub>9</sub>4-500-9 (1.68g/gcat-h in 4 hours reaction time). Longer reaction time allows for a longer contact time between catalyst and gas feedstock, thus giving more chance for decomposition of the carbon feedstock by the catalyst precursor during reaction.

Thirdly, reaction temperature shows a more significant effect towards the yield of CNF synthesized, compared to reaction time. For each of the three compositions of Fe-Ni in hybrid catalyst, the sample with the highest reaction temperature constantly yields the maximum amount of CNF synthesized; sample Fe<sub>14</sub>-600-3 for Fe-Ni ratio of 1/9, sample Fe<sub>5</sub>3-600-5 for Fe-Ni ratio of 5/5, and sample Fe<sub>9</sub>2-600-7 for Fe-Ni ratio of 9/1. At high temperatures, the process is more likely to have higher kinetic energy thus more collision (reaction) between the molecules take place.

## 4.2. XRD Pattern

XRD patterns are taken for the structural characterization of the as synthesized CNF. The generated graphs were compared to the vast library of XRD system database, allowing for identifying the existing compounds within the produced specimen.

The following symbols are used to identify the components from each XRD graph:

- Graphite
- Nickel
- △ Iron Carbide
- ▲ Iron

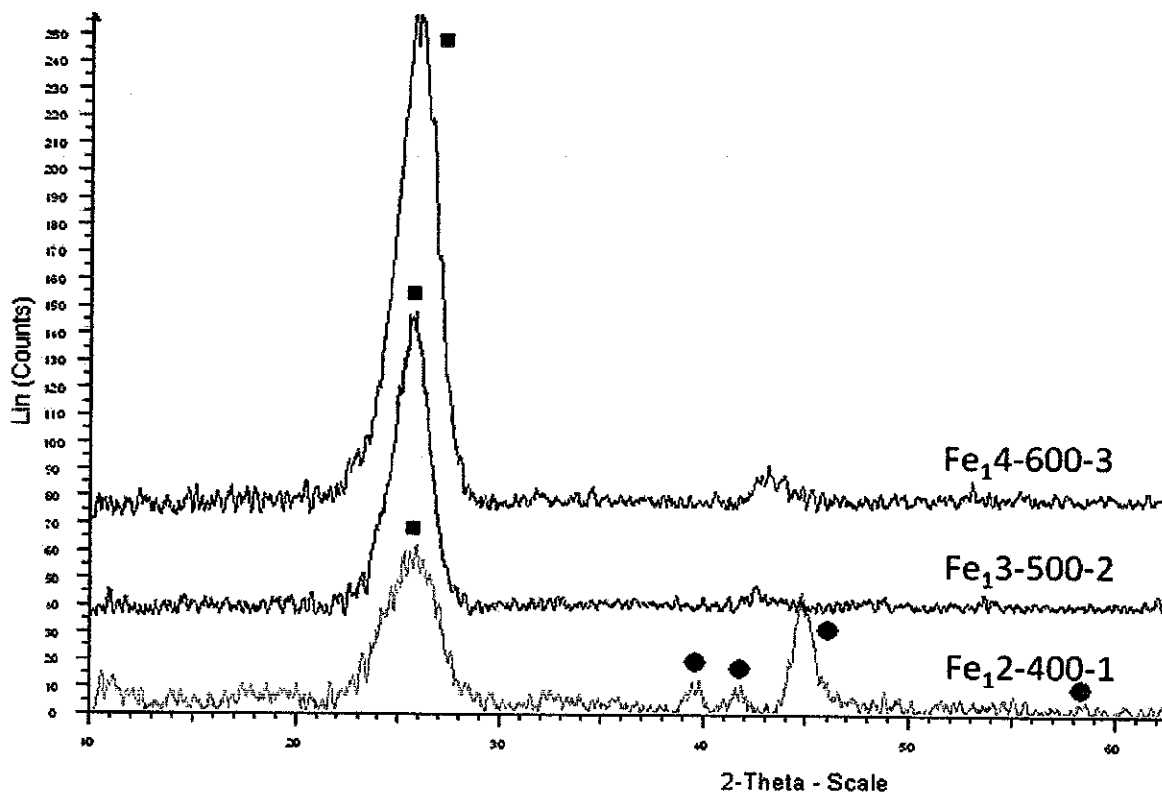


FIGURE 4.1: XRD Graph for Fe-Ni of 1:9

The above Figure 4.1 shows an XRD pattern for the first three samples using The Fe-Ni catalyst at a ratio of 1:9. Analysis of these patterns revealed that for all three samples, the peaks are explicable in terms of the known structure of graphite, where Fe<sub>14</sub>-600-3 is most



intense at its graphite peak. This is most likely due to its operating temperature, 600°C which is the maximum among the three. (Refer to **Appendix C, D & E** for a reference of XRD graph)

Fe<sub>2</sub>-400-1 noticeably gives a second peak which is identified as comparable with XRD of nickel, where the other two samples show no significant sign of the similar pattern, thus proving the idea of that low reaction time and operating temperature reduces the decomposition of carbon feedstock by the catalyst precursor. Traces of Ni, reduced from NiO, are still detectable at such operating conditions.

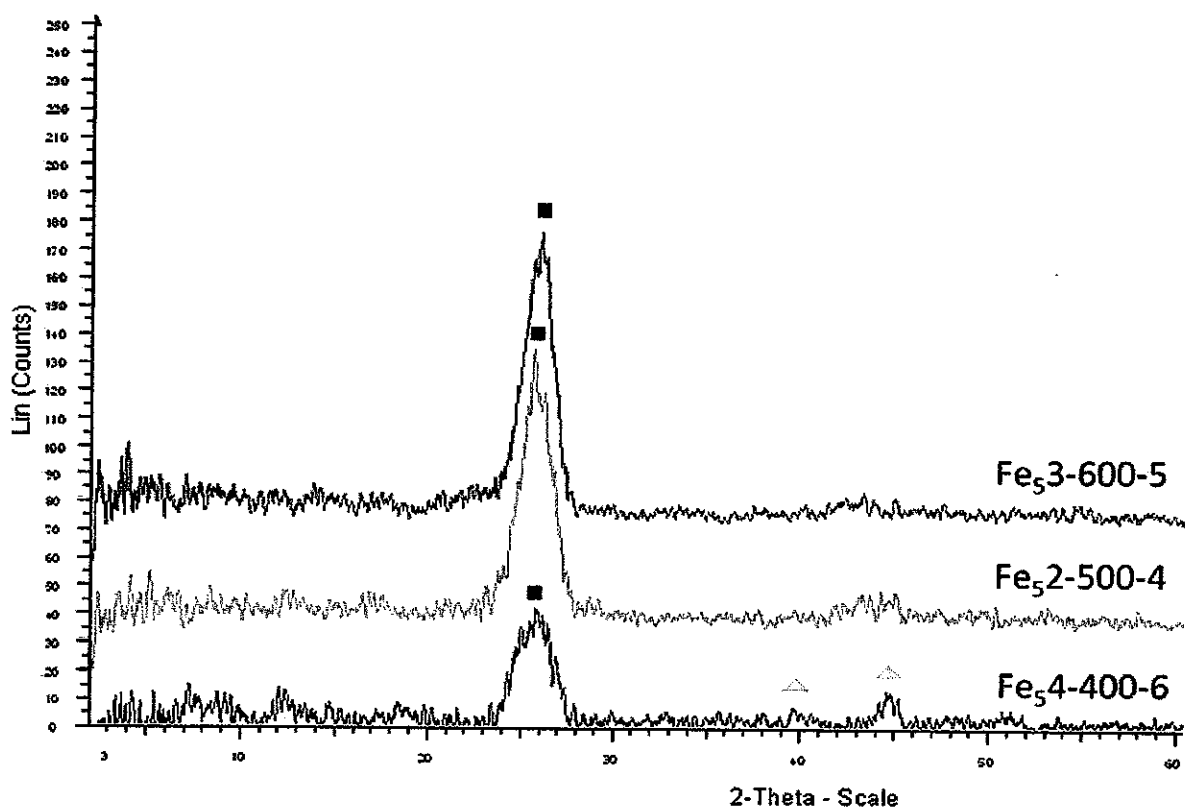


**FIGURE 4.2:** XRD Graph for Fe-Ni of 1:1

Samples #4, #5 and #6 are different of the previous set in terms of catalyst composition. Figure 4.2 shows the CNF samples of which the ratios between Fe-Ni are all 1:1 or 50% Fe 50% Ni each. A significant difference is that all three samples have almost the same intensity at peaks of graphite, with the highest temperature of 600°C producing the most.

Traces of both nickel and iron are also absent. Using a mixture of both catalyst precursors have maximized the conversion of carbon feedstock, thus only graphite material is detected.

As more  $\text{Fe}_2\text{O}_3$  catalyst precursor is used (Fe-Ni at 9:1), CNF is still produced, where graphite peaks are found in XRD image (Figure 4.3), however the intensity is much less compared to the previous samples. Fe-based catalyst favors more  $\text{H}_2$  and less  $\text{C}_2\text{H}_4$  in its gas feedstock mixture, where at a ratio of 1:1, only a high temperature of  $700^\circ\text{C}$  is practicable [McCaldin et al., 2006].

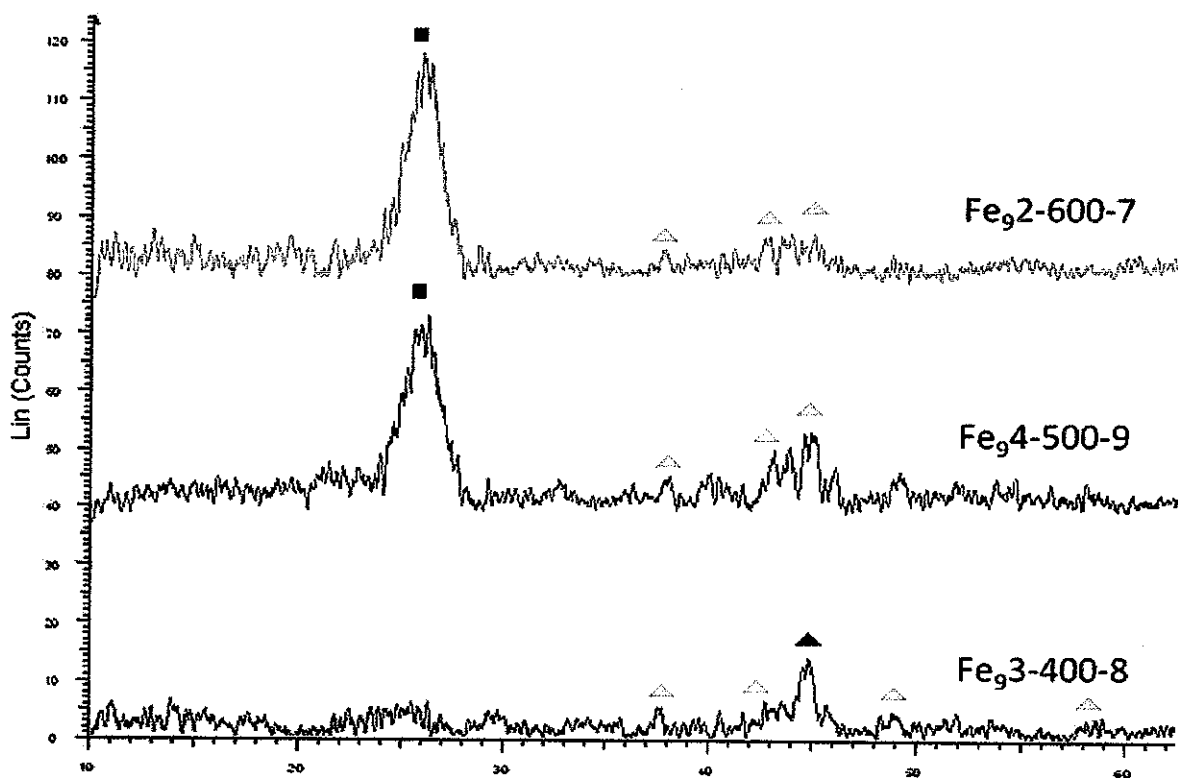
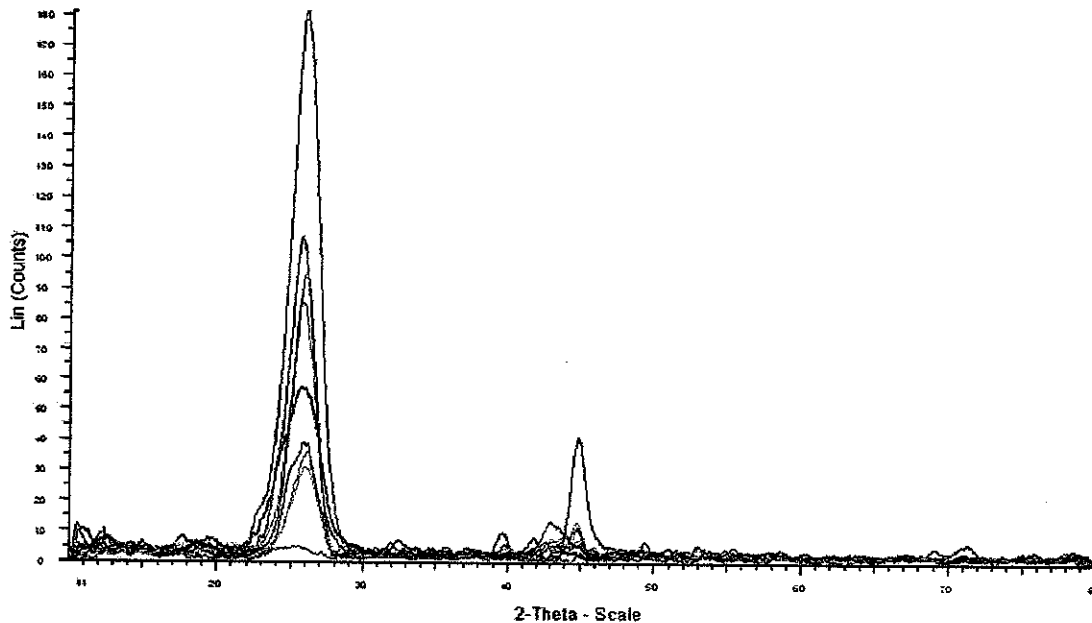


FIGURE 4.3: XRD Graph for Fe-Ni of 9:1

At  $400^\circ\text{C}$ , graphite is hardly detected; decomposition of gas feedstock is at its minimum, and the respective sample  $\text{Fe}_{93}\text{-}400\text{-}8$  produced the least yield ( $0.50 \text{ g/g}_{\text{cat}} \text{ h}$ ) of CNF product after 3 hours of reaction.  $\text{Fe}_{94}\text{-}500\text{-}9$  showed a most similar peak to the iron compound.

At the particular operating condition,  $\text{Fe}_2\text{O}_3$  is most likely reduced to Fe and  $\text{Fe}_3\text{C}$ , however the gas feedstock ratio does not permit for a high decomposition to produce CNF.



**FIGURE 4.4:** XRD image of all CNF sample

The above XRD image is of all the samples. As discussed earlier, the highest peak is of sample  $\text{Fe}_{14-600-3}$ , where the maximum operating conditions is in place. The lowest peak is of sample  $\text{Fe}_{93-400-8}$ .

### 4.3. Microstructural features of CNF

Electron microscopes are highly practicable to study the microstructures of the CNF sample, which has the features of a nano-scale range. The study includes that of SEM and TEM images.

#### 4.3.1. SEM

SEM micrographs are taken to study the surface morphology of the structures. Comparing to a TEM equipment, SEM images are not as high in resolution, where the maximum it can go is 1 nanometer (1 nm) [Blackman, 2005].

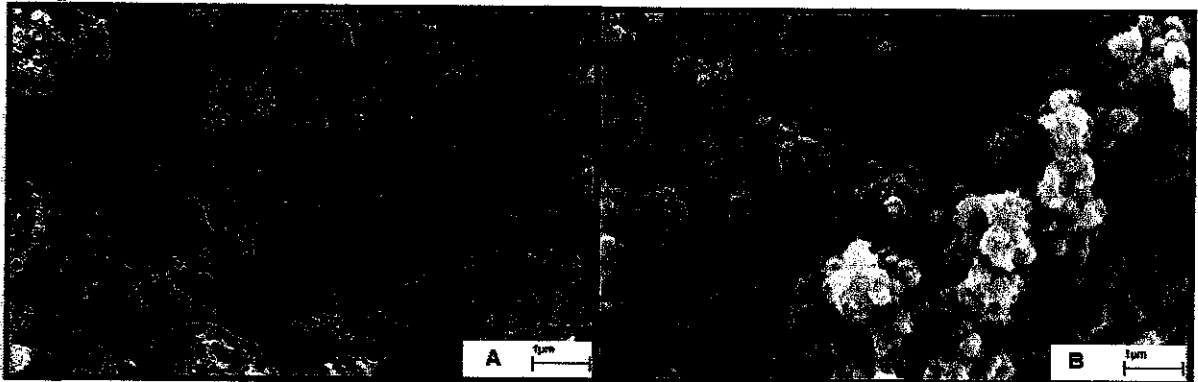


**FIGURE 4.5:** SEM image for (A)  $Fe_{14}$ -600-3 and (B)  $Fe_{93}$ -400-8 at 10kX

Figure 4.5 is a comparison of surface morphology for (A) maximum yield of CNF for  $Fe_{14}$ -600-3 at 44.6 g/  $g_{cat}$  h and (B) minimum yield of CNF for  $Fe_{93}$ -400-8 at 0.50 g/  $g_{cat}$  h. The difference in temperature is significantly the factor of the opposite output image. For  $Fe_{14}$ -600-3 operating at 600°C resulted in a spiral coil structures, which are the tubular shapes of a CNF, as discussed by Teo et al. [2003].  $Fe_{93}$ -400-8 operates at a temperature of 400°C, where a block of spherical compounds are identified instead of the cylindrical tubular structures. At 400°C, carbon is obviously not deposited to the other facet of the catalyst, thus no growth CNF occurs.

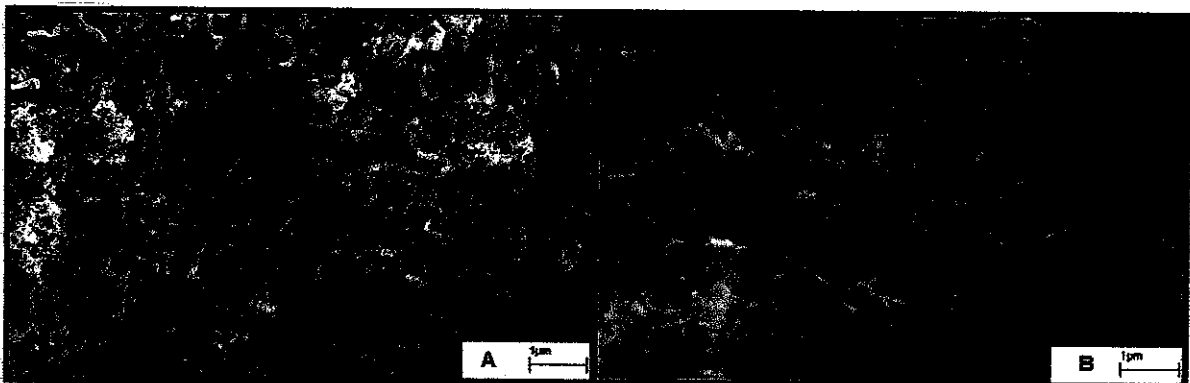


**FIGURE 4.6:** SEM image for (A)  $Fe_{13}$ -500-2 and (B)  $Fe_{52}$ -500-4 at 10kX

In Figure 4.6, the samples with physically most noticeable CNF growth are captured. Both samples  $Fe_{13}$ -500-2 and  $Fe_{52}$ -500-4 have similar operating temperatures of 500°C.

Bououdina et al. [2005] reported the maximum growth of CNF at 500°C, when the catalyst precursor is Ni-based, comparable to the results obtained by the author from this research. Both samples #2 and #4 have 90% and 50% composition of nickel catalyst respectively.

The micrographs above were magnified up to 10000X, but for a better feature identification of the structures, the following SEM image is captured at 25000X magnification, which is the maximum the particular SEM equipment would allow for a clear image.

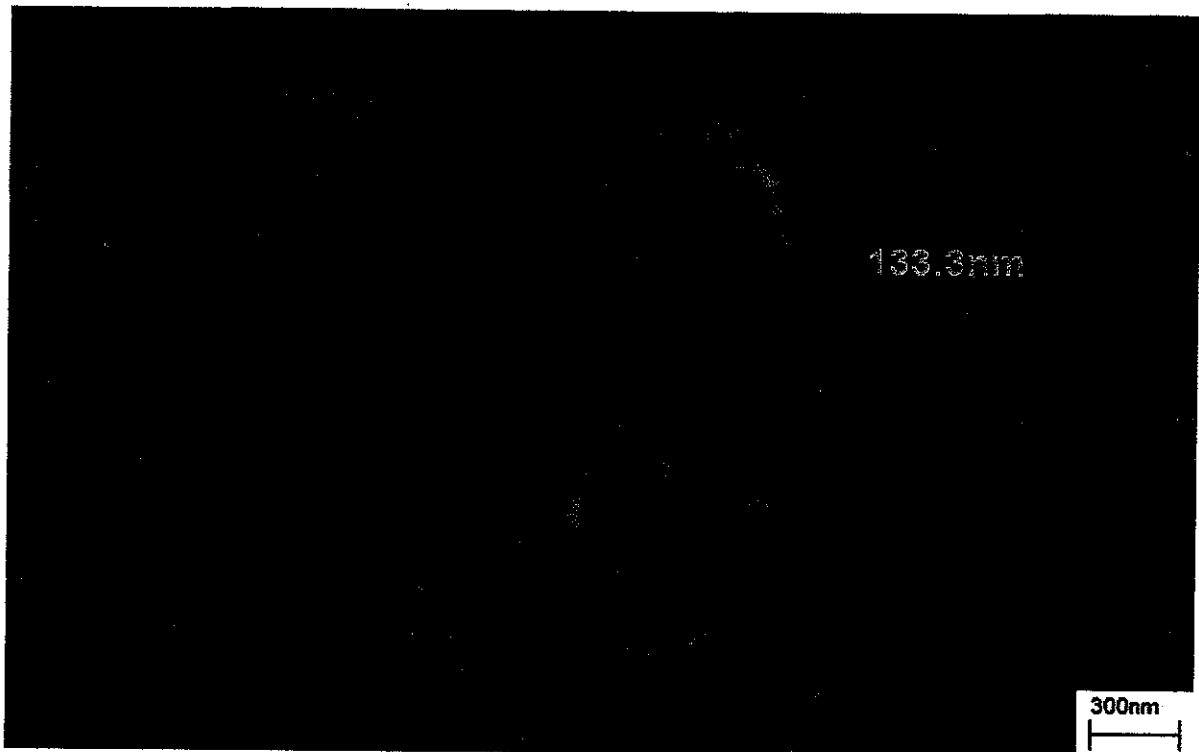


**FIGURE 4.7:** SEM image for Fe<sub>14</sub>-600-3 at 25kX

A 25k X magnification SEM micrograph of Fe<sub>14</sub>-600-3 is shown in Figure 4.7, where the smallest identified CNF cylindrical structure has a diameter of 26.7nm, and the biggest is 133.3nm. Any further magnification beyond 25k X resulted in blurry images, thus increasing difficulty to read the accurate diameter of each structure. The following table summarizes the diameter range of each nine samples identified from their respective SEM images:

**TABLE 4.2:** Diameter of CNF formed from Fe-Ni catalyst

Sample Name	Fe-Ni Composition	Reaction Time (hour)	Temp. (°C)	Graphitic Structure	Diameter, $\Phi$ (nm)
Fe <sub>1</sub> 2-400-1	1/9	2	400	No	-
Fe <sub>1</sub> 3-500-2	1/9	3	500	Yes	70-140
Fe <sub>1</sub> 4-600-3	1/9	4	600	Yes	30-130
Fe <sub>5</sub> 2-500-4	5/5	2	500	Yes	40-100
Fe <sub>5</sub> 3-600-5	5/5	3	600	Yes	30-140
Fe <sub>5</sub> 4-400-6	5/5	4	400	No	-
Fe <sub>9</sub> 2-600-7	9/1	2	600	Yes	100-260
Fe <sub>9</sub> 3-400-8	9/1	3	400	No	-
Fe <sub>9</sub> 4-500-9	9/1	4	500	Yes	40-80

Table 4.2 above demonstrates the diameter for each of the sample produced. For a Ni-based (90% Ni-composition) catalyst, the trend of diameter is quite simple; at high temperature, the diameter range starts to become smaller. Teo et al. [2003] discussed that “tubular structures ~20nm or below in diameter are nanotubes, but larger diameter filaments are nanofibers”. Nanotubes or more crystalline structures with more uniform graphene layers have a higher tendency to be produced along the growth axis when CVD process is operated at high temperatures of 700°C and above, thus explaining the decrease of diameter range for Fe<sub>1</sub>4-600-3 as the temperature approaches 700°C.

CNF produced from a 1:1 ratio composition also exhibit the same trend, Fe<sub>5</sub>3-600-5 operating at 600°C has a smaller minimum diameter of 30nm. Its maximum diameter is however 140nm, the incoherent trend most probably due to a mixture of both iron and nickel catalyst at the same composition.

For a Fe-based catalyst, the smaller diameter range is spotted at 500°C for Fe<sub>9</sub>4-500-9 with a diameter range of 40-80nm, compared to Fe<sub>9</sub>2-600-7 operating at 600°C of which the diameter is 100-260nm. The large diameter is due to the short reaction time of only 2 hours, where the CNF growth is still in development, and more time is required to form finer CNF.

Comparing Fe<sub>13</sub>-500-2 and Fe<sub>94</sub>-500-9, both operates at 500°C, the latter however displays a much smaller diameter of 40-80nm (against 70-140nm). This shows that Fe-based catalyst, although yields lower amount of CNF produced, have a tendency to produce smaller CNF structures, which is one of the preferable characteristics for an optimized CNF with large total surface area.

#### 4.3.2. TEM

TEM provides higher resolution micrographs of microstructures, yielding the sample's morphology and crystallography, and is able to detect atomic scale in areas of a few nanometers [Blackman, 2005]

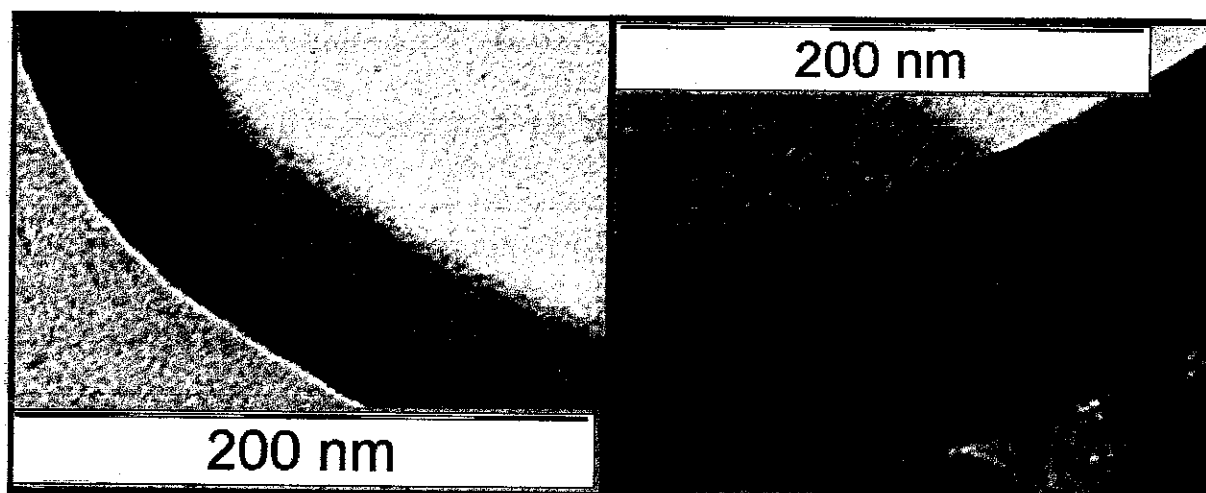
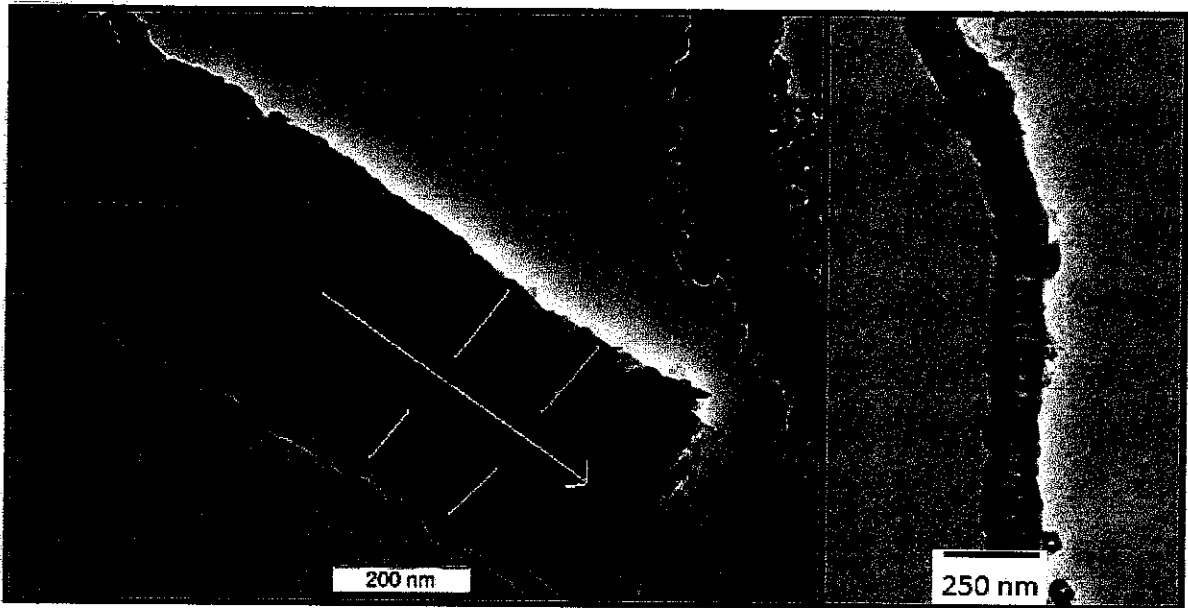


FIGURE 4.8: TEM image of Fe<sub>52</sub>-500-4

Both figures are from Fe<sub>52</sub>-500-4, operating with 1:1 ratio of Fe-Ni catalyst at 500°C for 2 hours. The green coloured line was drawn on the images to show the bone pattern of CNF produced, in which it exhibits a herringbone structure. McCaldin et al. [2006] reported that CNF produced at 500°C had a herringbone structure, which starts to develop to Platelet CNF when the operating temperature is 600°C. The latter can be seen from the following figures:



**FIGURE 4.9:** TEM image of Fe<sub>92</sub>-600-7

Figure 4.9 is a proven micrograph of a platelet CNF structure, where the graphene layers of the CNF are vertical to its axis, as compared to the studies by Zhou et al. [2006]. Referring to the studies by McCaldin et al. [2006], high temperatures favors the development of platelet CNF against that of herringbone.

Apart from that, encapsulation is also another event that occurs at high operating temperatures, usually 700°C and above. In sample Fe<sub>92</sub>-600-7, encapsulation can already be observed at a portion of the TEM image in Figure 4.10.



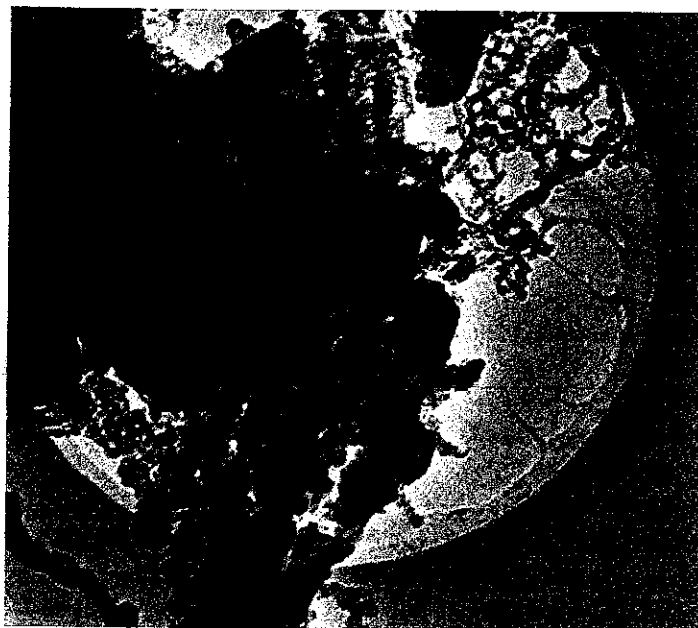


**FIGURE 4.10:** Encapsulation of catalyst at 600°C for Fe<sub>92</sub>-600-7

Only 2 samples were scanned under TEM due to unavailability of the equipment. The image however already proves that CNF can be generated when using hybrid compositions of catalyst, such in the case for Fe<sub>52</sub>-500-4. Although high reaction temperature tends to produce higher yield of CNF, events of encapsulation must also be considered, since encapsulation blocks entry of gasses, thus significantly reduces gas storage, which is against the objective of this research. Further assessment of the sample's total surface area and the amount of adsorption it gives is necessary to identify the most optimum CNF structure for hydrogen storage purposes. Previous results of high CNF yield when using Ni-based catalyst also does not mean it is fully optimized, thus requiring more studies and comparison between the samples.

#### 4.4. Chemical Composition of CNF

The information on particle composition and morphology is extremely useful for understanding the makings of a component or specimen. Based on these properties itself, characteristics such as the expected life or the quality of the component can be recognized.

Such information is available with the use of a SEM-EDX, and extended function of a scanning electron microscopy, which is the energy-dispersive X-ray spectroscopy. EDX analysis conducted by means of a SEM is able to determine the chemical composition of a specimen.

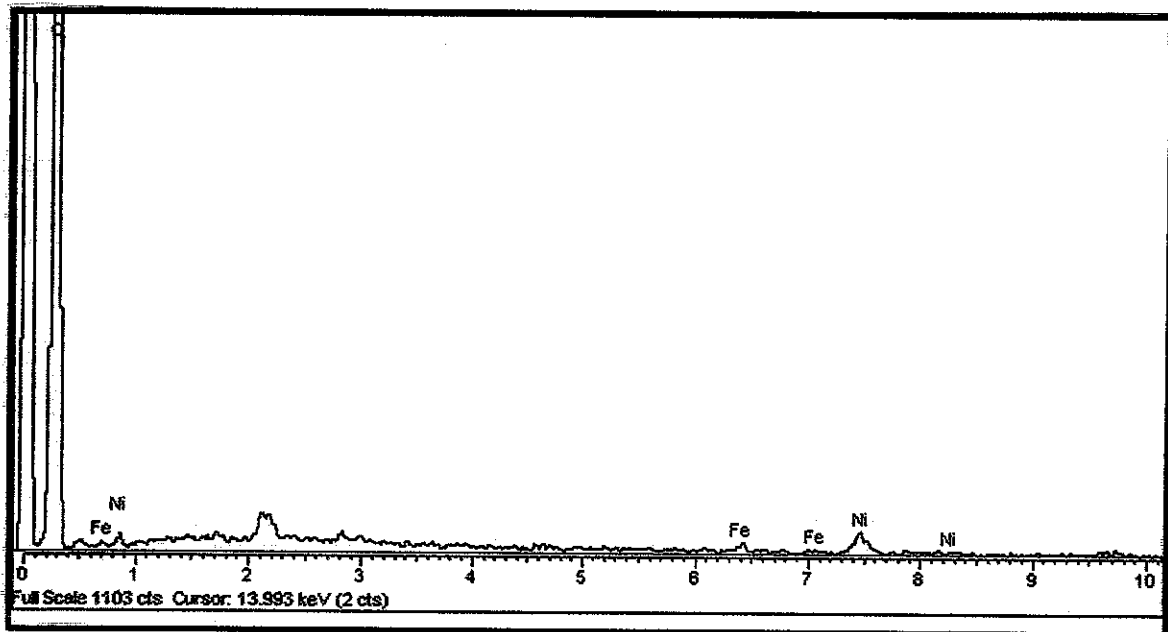


FIGURE 4.11: Different compositions of CNF Fe<sub>5</sub>2-500-4

From the above figure for sample Fe<sub>5</sub>2-500-4, the first two peaks are of the carbon component, showing that the CNF produced is mostly consist of carbon material. In this case, the metal precursors which are nickel and iron are almost untraceable, since carbonaceous gas feedstock had deposited carbon on the metal facet, and further diffusion of the carbon produces CNF on the other facet of the metal catalyst.

Four components basically exist in the CNF structure, consisting of carbon (C), monoxide (O), nickel (Ni) and iron (Fe). Thus the result is reviewed based on the percentage for each of these components in the CNF produced:

**TABLE 4.3: Weight percent of CNF composition**

Weight %:	Carbon (C)	Oxide (O)	Nickel (Ni)	Iron (Fe)
Fe <sub>1</sub> 2-400-1	91.92	5.58	2.50	0
Fe <sub>1</sub> 3-500-2	93.97	4.99	0.50	0
Fe <sub>1</sub> 4-600-3	94.11	5.89	0	0
Fe <sub>5</sub> 2-500-4	97.22	0	2.23	0.55
Fe <sub>5</sub> 3-600-5	93.56	5.50	0.94	0
Fe <sub>5</sub> 4-400-6	92.65	4.91	2.44	0
Fe <sub>9</sub> 2-600-7	91.43	7.49	0	1.08
Fe <sub>9</sub> 3-400-8	90.49	0	5.79	3.72
Fe <sub>9</sub> 4-500-9	86.46	7.83	1.99	3.72

For samples Fe<sub>1</sub>2-400-1, Fe<sub>1</sub>3-500-2 and Fe<sub>1</sub>4-600-3, carbon component increases when CNF is produced at higher temperatures and reaction time. This is the pattern when nickel is the precursor catalyst. Along the same change of operating conditions, nickel composition decreases until all traces are gone at 600°C after 4 hours of reaction time. Thus carbon is fully decomposed on the catalyst facet. The hybrid catalyst for these samples only contains 10% of iron, thus no traces are found even at the low operating conditions.

The more interesting result would be for sample Fe<sub>5</sub>2-500-4, Fe<sub>5</sub>3-600-5 and Fe<sub>5</sub>4-400-6 of which the catalyst precursor is 50%-50% for nickel-iron. Maximum carbon formation is identified at 500°C after only 2 hours of reaction time. Nickel shows a very dependant trend against temperature, where least amount is identified at higher temperatures. Comparing nickel and iron, at the same composition of the catalyst, carbon easily decomposes on iron metal, since traces of iron quickly lessens. The only trace of iron is detected when the reaction time is low after only 2 hours.

Samples Fe<sub>9</sub>2-600-7, Fe<sub>9</sub>3-400-8 and Fe<sub>9</sub>4-500-9 will mostly reflect the trend for iron precursor, since its composition in the hybrid catalyst is 90%. The same trend is seen for formation of carbon and reduction of nickel component, which is temperature dependant. At 600°C, iron also reduces due to decomposition and diffusion of carbon through the metal. However, 1.08% of iron still exists, which is mostly due to the low reaction time. This strengthens the conclusion that the reduction of iron is more dependent on longer reaction times as opposed to only reaction temperature.



**FIGURE 4.12:** Produced CNF in bulk powder form

Based on literature study, CNF structure development differs between using NiO and Fe<sub>2</sub>O<sub>3</sub> catalyst, with respect to different carbonaceous gas feedstock composition. In the case of using NiO as the precursor, CNF with graphitic structure are formed even at a high ratio of C<sub>2</sub>H<sub>4</sub> to hydrogen, for example 80:20 (total of 100sccm) at higher temperatures. Fe<sub>2</sub>O<sub>3</sub> catalyst however shows a different trend where high C<sub>2</sub>H<sub>4</sub> ratio easily forms encapsulation at higher temperatures. Graphitic structures of CNF are mostly formed at lower C<sub>2</sub>H<sub>4</sub> ratios when using Fe<sub>2</sub>O<sub>3</sub> as the precursor.

Both catalyst precursors show a same trend with respect to temperature, where herringbone CNF structure is likely to form at lower temperatures of 350-500°C, while platelet CNF structure forms when the temperature is set around 500-700°C. As reported by McCaldin et

al., [2006] very high temperatures around 700-800°C will usually cause encapsulation of the catalyst, where no graphitic structure is formed. This is proven by the author's result of sample Fe<sub>9</sub>2-600-7 where the TEM image showed traces of encapsulation.

#### 4.5. Main Effect on CNF Yield

The following graph represents the trend of each factor towards the yield of the CNF produced.

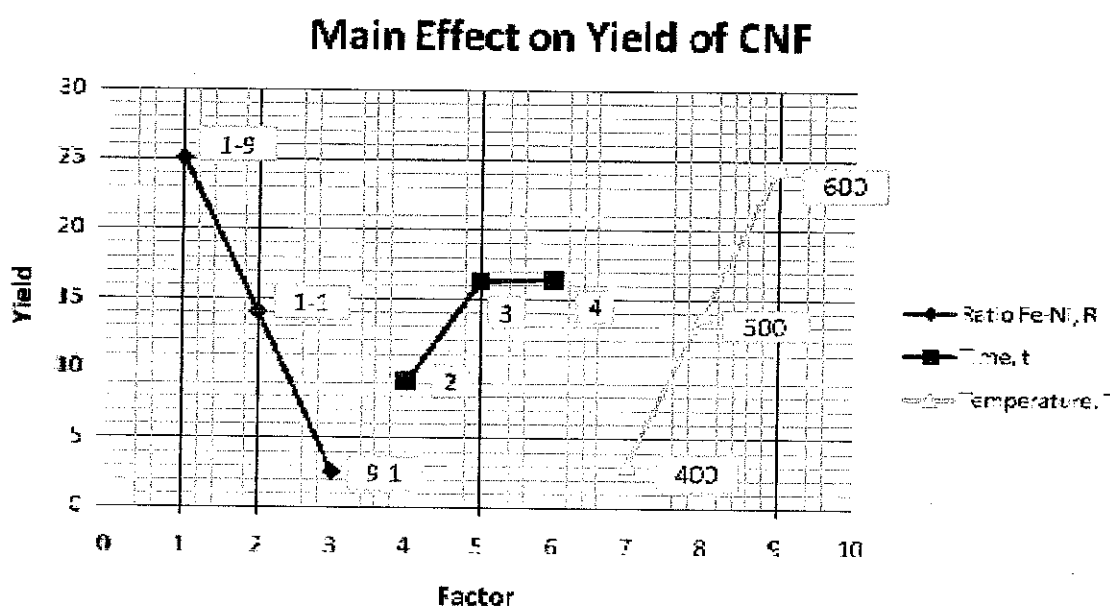


FIGURE 4.13: Main effect on yield of CNF

Based on the plot, maximum yield (characteristic: “the bigger the better”) is achieved by having the maximum; (i) ratio of nickel catalyst, (ii) reaction time and (iii) reaction temperature. Thus the optimum condition is 10% Fe 90% Ni in catalyst, 4 hours and 600°C. The trend shows small effect on yield when varying the time between 3-4 hours, but very significant changes when varying catalyst composition and reaction temperature.

#### 4.6. Percent Contribution

Taguchi Method includes the analysis of variance (ANOVA), a statistically based tool for detecting any differences in average performance of groups of items tested [Ross, 1996].

Among the benefits is that the contribution, or degree of effect of a particular factor towards the experiment can be determined.

**TABLE 4.4: Analysis of Variance**

Source	DOF	SS	V	F	SS'	P
Catalyst Ratio, Fe/Ni	2	760.96	380.48	4.22	580.57	33.40
Time	2	107.06	53.53	0.59	-73.33	-4.22
Temperature	2	689.87	344.93	3.82	509.48	29.31
Error, e	2	180.39	90.19	1.00	721.56	41.51
Total	8	1738.27				100

The contribution factor can be analysed from the variance, V, or more effectively the percent contribution, P. From the ANOVA table, the calculation showed that ratio of Fe-Ni is the most dominant factor, as it is most sensitive to variation of its level. Following after is the reaction temperature, while reaction time has the least contribution percent. This agrees with the trend from the plot of main effects of each factor in Chapter 4.5. Thus ratio of catalyst is the important item to control, including reaction temperature.

Percent contribution due to error is less than 50%, thus theoretically no important factors were omitted from the experiment. However, the value almost reaches the high percent of 50%. This shows that it is possible that some important factors might have been omitted or some conditions might not be precisely controlled. Thus, there is opportunity for further improvement and experimentation. In other words, another important factor such as the ratio of gas composition should be studied together.

From the most contributing factor, nickel forms high yield of CNF, but it is not necessary that the CNF has high capacity of hydrogen storage. Apart from CNF yield, the same analysis of main effects and percent contribution should also be reviewed in terms of CNF surface area and hydrogen adsorption, once the result data is available.

## CHAPTER 5

### COST ESTIMATION

The important raw materials used for the experiment are basically hydrogen gas, ethylene gas feedstock, iron (III) oxide and nickel oxide catalyst

Based on the maximum yield of CNF produced which is 44.60 g/g<sub>cat</sub>.hr, the yield is approximately 10g in 4 hours, using 0.045g of nickel and 0.005g of iron precursors.

Price of Ethylene = RM1430/12.3m<sup>3</sup>

Price of Hydrogen = RM386.48/7.2m<sup>3</sup>

Price of Iron Catalyst = RM 274.24/500g

Price of Nickel Catalyst = RM452.97/500g

For 4 hours of reaction time, the CNF produced is approximately 10g. Thus, the cost for producing 10g of CNF is:

Cost of Ethylene = RM4.18/0.036m<sup>3</sup>

Cost of Hydrogen = RM1.93/0.036m<sup>3</sup>

Cost of Iron Catalyst = RM 0.0027/0.005g

Cost of Nickel Catalyst = RM0.0408/0.045g

Total Cost = RM 6.1535/10g of CNF

= RM 615.35/kg of CNF

Based on research on the market price, commercial CNF is available from Pyrograf Products Inc. at a price of \$85/pound, which is equal to approximately RM 674.43/kg of CNF.

Thus, comparatively, the production cost which includes the cost of raw materials alone is lower than the commercial price. At higher production, the overall cost should be lower per each kg, thus the project is feasible.

## CHAPTER 6

### CONCLUSION & RECOMMENDATION

#### 6.1. Conclusion

Based on the analysis of the results, the yield of CNF synthesized is very dependent on the catalyst composition, reaction time and reaction temperature. Higher yield is obtained when more Nickel Oxide is used in the hybrid catalyst, longer reaction time takes place, and also as reaction is operated at higher temperatures.

Hybrid catalyst also resulted in successfully forming the graphitic structures of a CNF based on the graphite peaks in XRD, where herringbone CNF structures were identified from the TEM image. Based on the current results, Ni-based catalyst yields more CNF, but a mixture of both catalysts observed lower diameter ranges of CNF, a preferable characteristic for a higher surface area of CNF. The optimum value for catalyst ratio can only be optimized with the support of surface area and hydrogen adsorption data.

As a conclusion, operating conditions is at its best performance at 600°C and 4 hours of reaction time.



## 6.2. Recommendation

- Further analysis and characterization is vital to fully understand the reaction mechanism, and identify the optimum conditions that will produce CNF with the highest capacity for hydrogen storage. These analyses include identifying the total surface area and percent of gas adsorption for each sample.
- As a recommendation, it would be best to advance the experiment on CNF synthesis at different composition of gas feedstock, since both catalysts used favor different composition of  $C_2H_4$  and  $H_2$ .
- Although nickel catalyst precursors tend to produce more CNF yield, the price of iron catalyst is much cheaper, thus the hybrid catalyst is favorable to address both benefits. Contribution percent of catalyst ratio is also the largest. Therefore, it is suggested that the research on hybrid catalyst is continued.
- The current research studies also proved that higher BET surface area does have a proportional relation with the hydrogen adsorption capacity of a CNF structure in most cases. Therefore, high BET surface area is deemed as the objective for developing the CNF structures.
- For upcoming research, the temperature and reaction time is to be fixed at  $600^\circ C$  and 4 hours respectively. Other factors; Fe-Ni catalyst composition and  $C_2H_4$ - $H_2$  gas composition is to be varied.

## REFERENCES

1. Bououdina, M., Grant, D. and Walker, G., 2005 "Effect of processing conditions on unsupported Ni-based catalysts for graphitic-nanofibre formation", *Carbon* **43**: 1286-1292
2. Blackman, J.M., Patrick, J.W., Ana Arenillas, Wei Shi and Snape, C.E., 2006 "Activation of carbon nanofibres for hydrogen storage", *Carbon* **44**: 1376-1385
3. Gupta, B.K. and Srivastava, O.N., 2000 "Synthesis and hydrogenation behavior of graphitic nanofibres", *International Journal of Hydrogen Energy* **25**: 825-830
4. McCaldin, S., Bououdina, M., Grant, D.M. and Walker, G.S., 2006 "The effect of processing conditions on carbon nanostructures formed on an iron-based catalyst", *Carbon* **44**: 2273-2280
5. Teo, K.B.K., Singh, C., Chhowalla, M. and Milne, W.I. 2003 "Catalytic Synthesis of Carbon Nanotubes and Nanofibers", *Encyclopedia of Nanoscience and Nanotechnology*: 1-22
6. Zhou, J.H., Sui, Z.J., Ping Li, De Chen, Dai, Y.C. and Yuan, W.K., 2006 "Structural characterization of carbon nanofibers formed from different carbon-containing gasses", *Carbon* **44**: 3255-3262
7. Duong D. Do 1998, *Adsorption Analysis: Equilibria and Kinetics*, London, Imperial College Press
8. Geankoplis C.J. 2003, *Transport Processes and Unit Operations*, 4th Edition, Prentice Hall
9. Deborah D.L. Chung 1994, *Carbon Fiber Composites*, United States, Butterworth-Heinemann
10. Ross, P.J., 1996, *Taguchi Techniques for Quality Engineering*, Singapore, Mc Graw-Hill

11. Peace G.S., 1993, *Taguchi Methods A Hands-On Approach*, USA, Addison-Wesley
12. Blackman, J.M., 2005, *High Pressure Hydrogen Storage on Carbon Materials for Mobile Applications*, Ph.D. Thesis, University of Nottingham, United Kingdom
13. Athirah Mohd Tamidi, 2008. *Development of Catalyst for Carbon Nanofiber*. FYP Progress Report, Universiti Teknologi Petronas, Perak, Malaysia
14. Tuinstra, F. and Koenig, J.L. 1969. *Raman Spectrum of Graphite*, Cleveland, Case Western Reserve University.
15. Roy, R.K. 1990. *A Primer on the Taguchi Method*, USA, Society of Manufacturing Engineers
16. <[http://commons.wikimedia.org/wiki/Image:Activated\\_Carbon.jpg](http://commons.wikimedia.org/wiki/Image:Activated_Carbon.jpg)>

APPENDICES

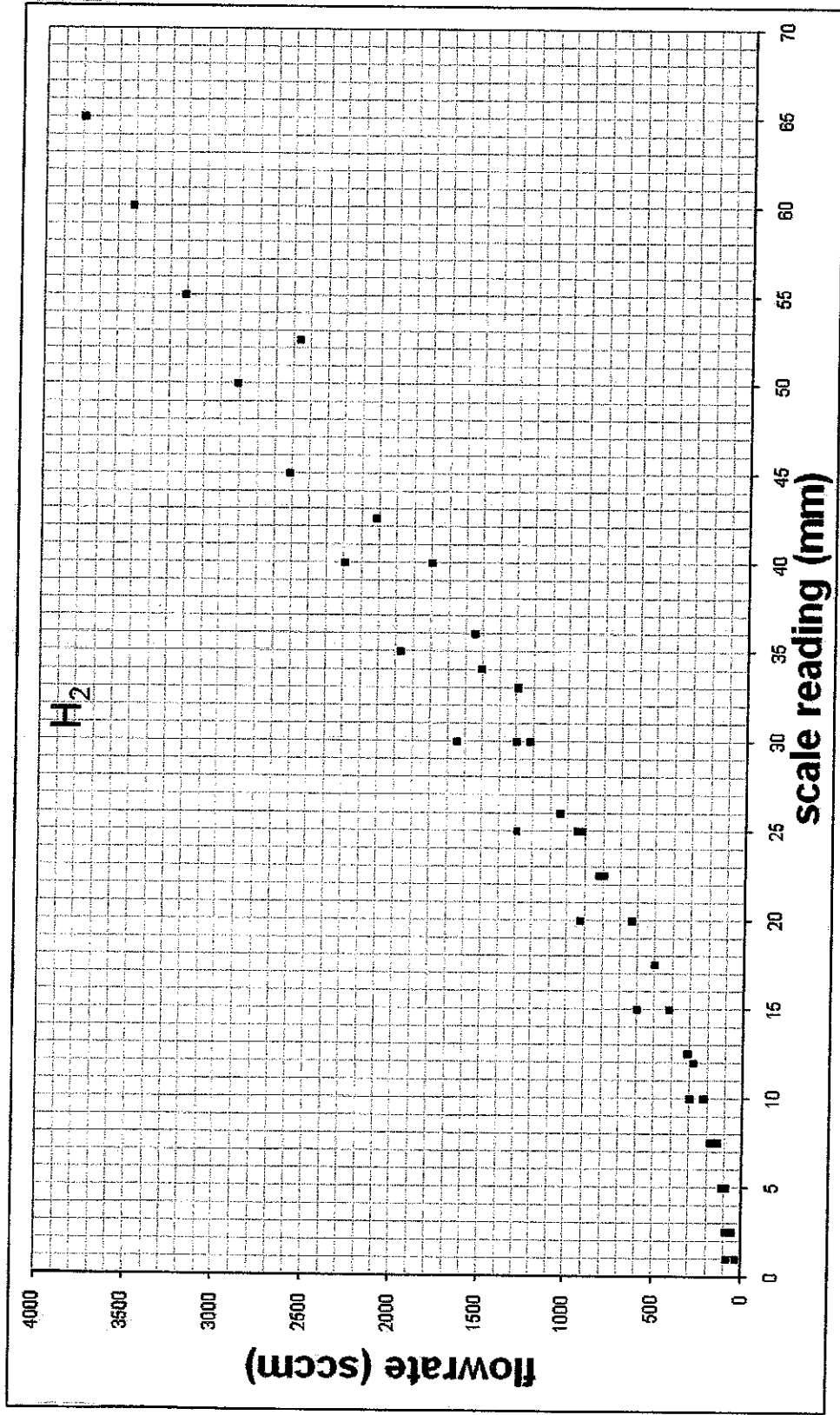


FIGURE A: Hydrogen scale in laboratory

Date	Sample Name	Gas		H2 Scale	Catalyst (ratio)	Cat (g)		Reaction		Mass w/o cat (g)		Boat + CNF (g)		Product mass (g)		Yield (g/ g cat hr)		
		ratio	flowrate			B1	B2	Time (hr)	Temp (°C)	B1	B2	B1	B2	B1	B2	B1	B2	Average
<b>CH<sub>4</sub>/N<sub>2</sub>:</b>																		
19/12/08	Trial #1	9/1	450/50		Fe <sub>2</sub> O <sub>3</sub>	0.0533	0.0551	3	500					0	0	0.00	0.00	0.00
22/12/08	Trial #2	5/5	250/250		Fe <sub>2</sub> O <sub>3</sub>	0.0534	0.0520	3	700	109.2500	98.16	109.25	98.16	0	0	0.00	0.00	0.00
23/12/08	Trial #3	1/9	50/450	12.5	1/Fe 2/Ni	0.0558	0.0537	3	700	119.3098	113.1983	119.3497	113.2699	0.0399	0.0716	0.24	0.44	0.34
<b>CH<sub>4</sub>/N<sub>2</sub>:</b>																		
24/12/08	Ni-2.5.4-1	1:1	250/250	10.5	NiO	0.0550	0.0585	2	400	OL	104.99	OL	105.5623	0.7673	0.5723	6.98	4.89	5.93
<b>Start of Hybrid Catalyst:</b>																		
<b>Fe<sub>3</sub>/Ni</b>																		
2/1/09	Fe <sub>2</sub> -400-1	1:1	200/200	9.5	1/9	0.0507	0.0510	2	400	OL	119.3106	OL	119.6706	0.6803	0.36	6.71	3.53	5.12
5/1/09	Fe <sub>3</sub> -500-2	1:1	150/150	8.5	1/9	0.0552	0.0530	3	500	109.2527	119.3109	115.1902	123.9964	5.9375	4.6855	35.85	29.47	32.66
6/1/09	Fe <sub>4</sub> -600-3	1:1	150/150	8.5	1/9	0.0561	0.0541	4	600	113.1960	104.9968	121.3238	113.1367	8.1278	8.1999	36.22	37.62	36.92
<b>Start of Hybrid Catalyst:</b>																		
30/1/09	Fe <sub>2</sub> -400-10	1:1	150/150	7.5	1/9	0.0591	0.0548	2	400	119.3110	104.994	120.1806	105.4829	0.8696	0.4889	7.36	4.46	5.91
31/1/09	Fe <sub>3</sub> -500-11	1:1	150/150	7.5	1/9	0.0570	0.0533	3	500	OL	114.215	OL	118.4901	3.93	4.2704	22.98	26.71	24.84
2/2/09	Fe <sub>4</sub> -600-12	1:1	150/150	7.5	1/9	0.0568	0.0522	4	600	113.1977	98.1597	123.5448	107.2739	10.3471	9.1142	45.54	43.65	44.60
10/1/09	Fe <sub>3</sub> -500-4	1:1	150/150	7.5	5/5	0.0530	0.0536	2	500	113.1949	98.1573	114.9485	99.7825	1.7536	1.5752	16.54	14.69	15.62
12/1/09	Fe <sub>3</sub> -600-5	1:1	150/150	7.5	5/5	0.0578	0.0530	3	600	119.3075	104.9935	123.4313	108.6985	4.1238	3.705	23.78	23.30	23.54
13/1/09	Fe <sub>4</sub> -400-6	1:1	150/150	7.5	5/5	0.0555	0.0523	4	400	113.1918	98.157	113.9626	98.6882	0.7708	0.5312	3.47	2.54	3.01
21/1/09	Fe <sub>2</sub> -600-7	1:1	150/150	7.5	9/1	0.0510	0.0505	2	600	113.1932	98.1553	113.7577	98.7291	0.5645	0.5738	5.53	5.68	5.61
22/1/09	Fe <sub>3</sub> -400-8	1:1	150/150	7.5	9/1	0.0509	0.0512	3	400	119.3157	104.9991	119.3928	105.0745	0.0771	0.0754	0.50	0.49	0.50
23/1/09	Fe <sub>4</sub> -500-9	1:1	150/150	7.5	9/1	0.0522	0.0515	4	500	113.2005	98.1624	113.5359	98.5225	0.3354	0.3601	1.61	1.75	1.68

FIGURE B: Raw Result Data Collection

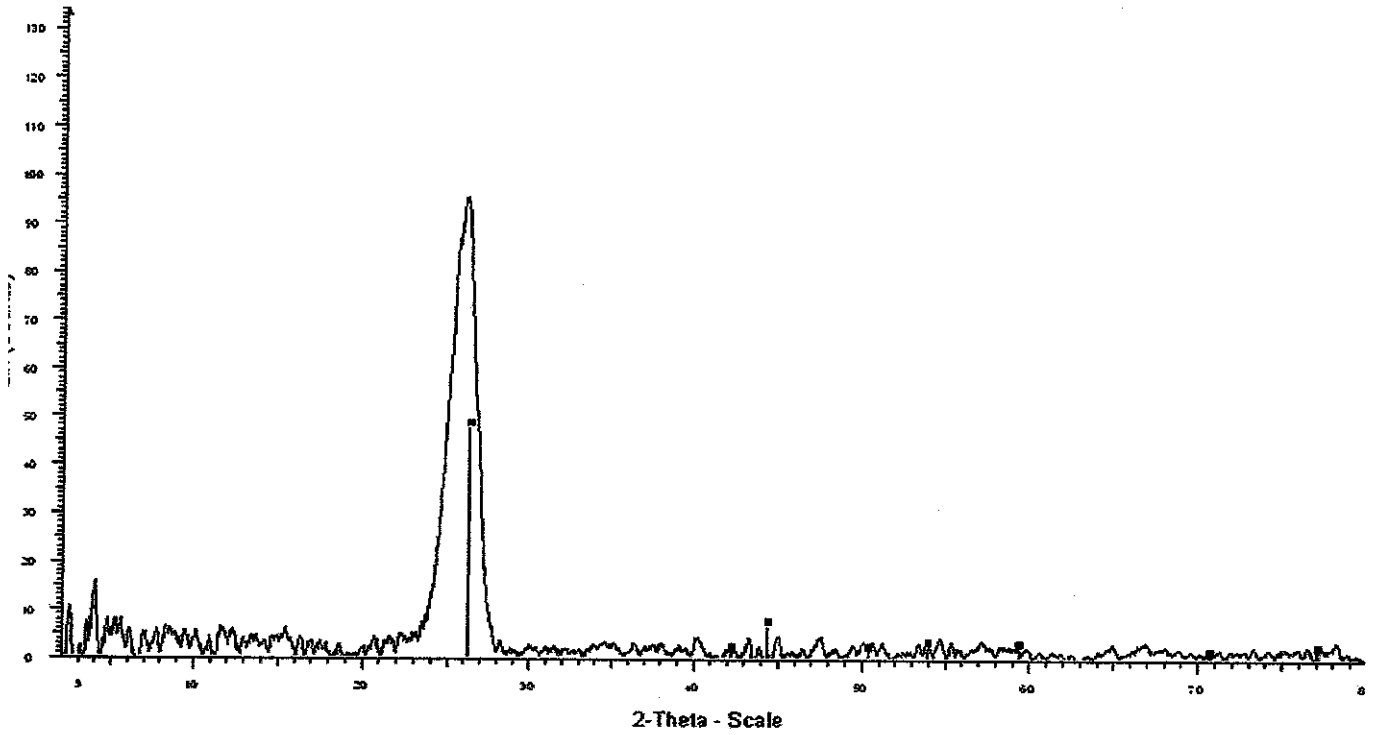


FIGURE C: XRD Reference for Graphite

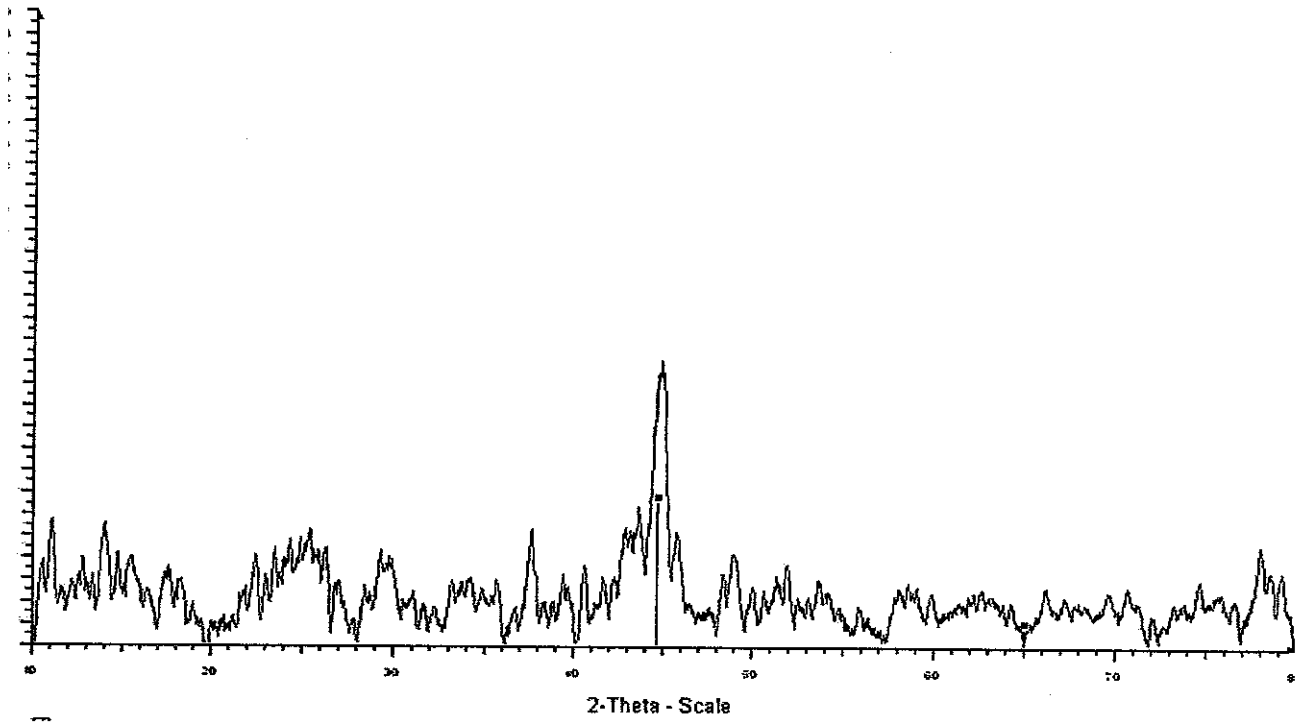


FIGURE D: XRD Reference for Iron (Fe)

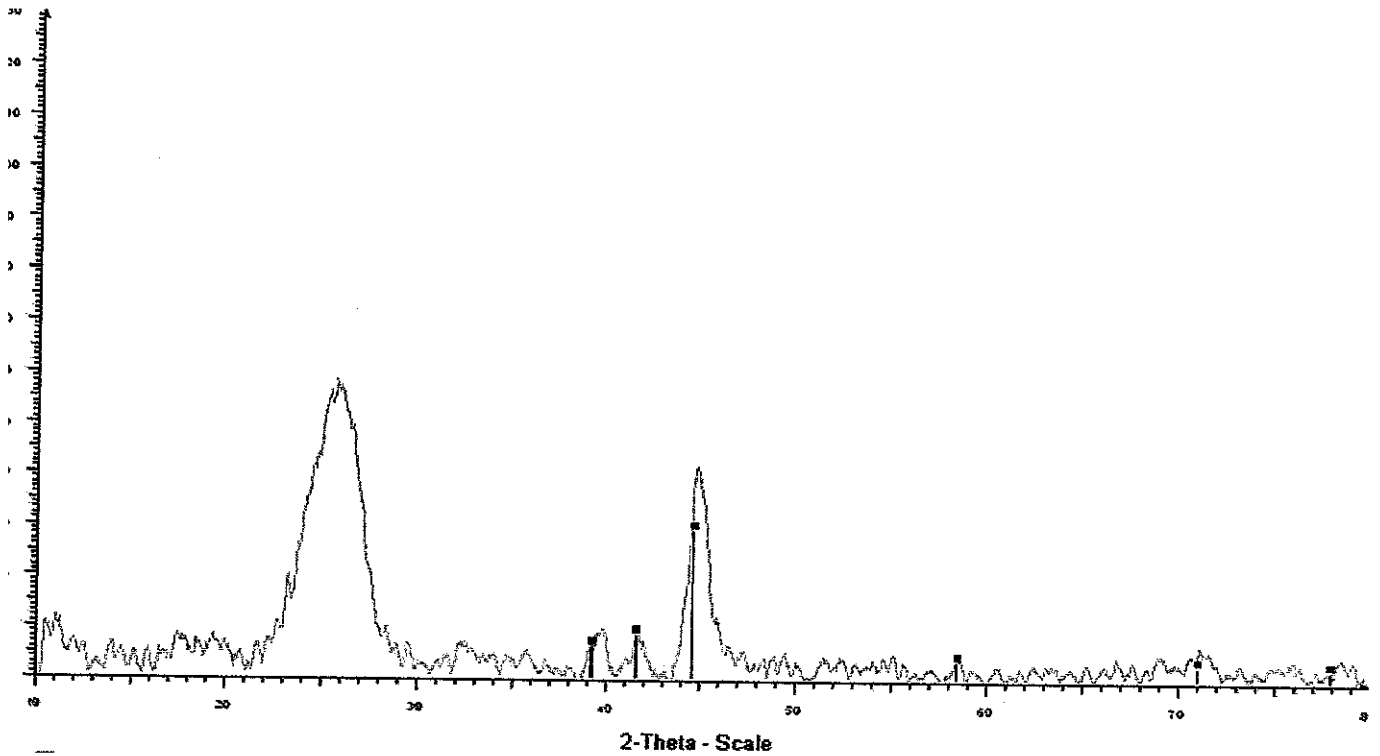


FIGURE E: XRD Reference for Nickel (Ni)

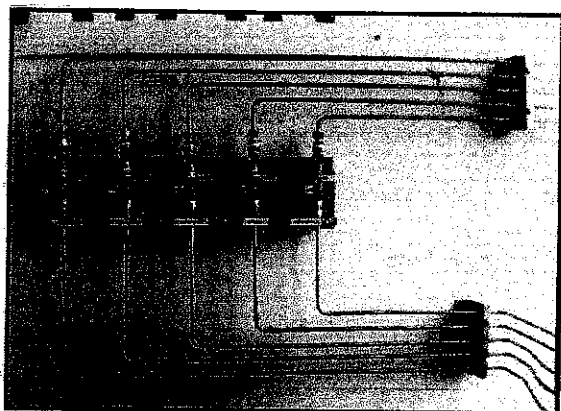


FIGURE F: Feed Gas Main Controller

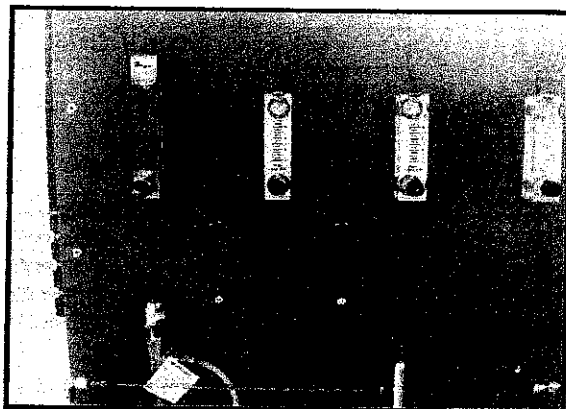


FIGURE G: Gas feedstock Valve Controller



FIGURE H: Horizontal Tubular Reactor

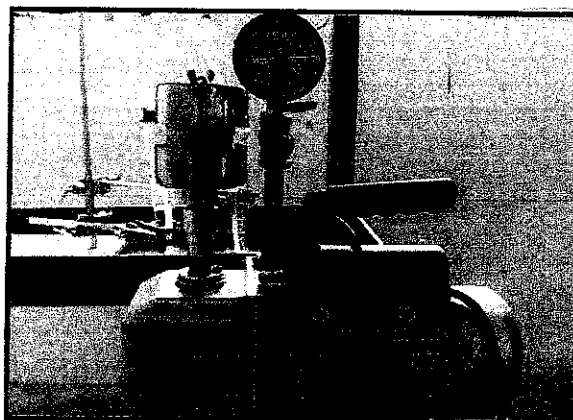


FIGURE I: Pressure Gauge/ Vacuum Pump



Spectrum processing:

Peak possibly omitted: 2.142 keV

Processing option: All elements analyzed (Normalised)

Number of iterations = 4

Standard:

C CaCO3 1-Jun-1999 12:00 AM

Fe Fe 1-Jun-1999 12:00 AM

Ni Ni 1-Jun-1999 12:00 AM

Element	Weight%	Atomic%
C K	97.22	99.41
Fe K	0.55	0.12
Ni K	2.23	0.47
Totals	100.00	

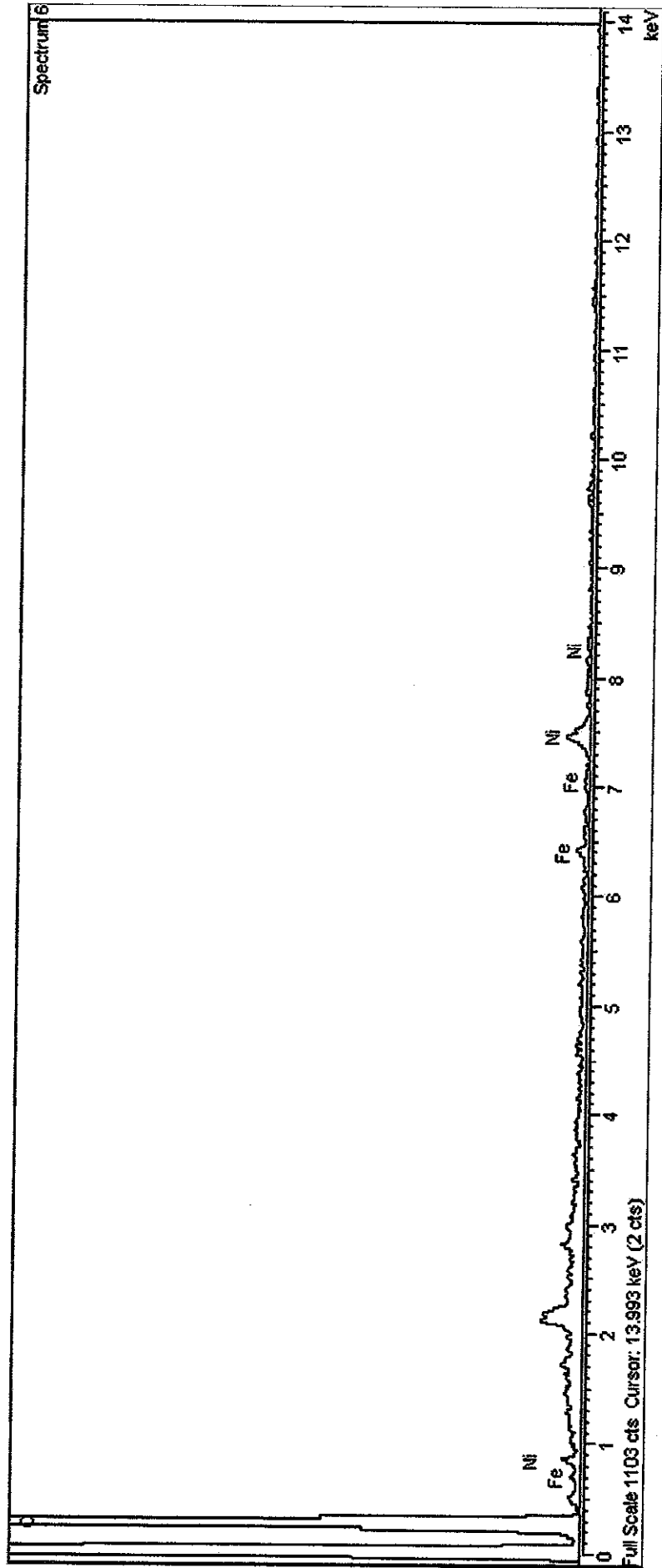


FIGURE J. EDX Graph